Environmental Applications of Magnetron Sputter Coated Coal Fly Ash

A H GADDAH

PhD 2023

Environmental Applications of Magnetron Sputter Coated Coal Fly Ash

Abdul Hadi Gaddah

A thesis submitted in partial fulfilment of the requirements of Manchester Metropolitan University for the degree of Doctor of Philosophy

Department of Engineering, Manchester Metropolitan University

2023

Acknowledgments

Firstly, I would like to thank my director of studies Professor Peter Kelly, for his patience with me on this journey and his guidance and support throughout the PhD. Secondly, I would like to thank the team that helped carry this PhD, my supervisors, Dr Marina Ratova and Professor Herman Potgieter, along with the technicians at Manchester Metropolitan University, in particular Dr Gary Miller and Mrs Hayley Andrews. Their input, support and guidance were crucial in driving the research to the point it has reached and achieving its aims.

I would like to express my sincere appreciation and recognition for the work carried out by Professor Herman Potgieter's Masters students in conducting experiments and analysis using the TiO_2 coated flyash. Furthermore, I am truly grateful for the collaboration opportunity presented by Professor Herman Potgieter. The work helped provide confidence in the novelty of the research.

This journey I embarked on was a once-in-a-lifetime experience with ups and downs to overcome. Deciding to start this PhD part-time was challenging as funds needed to be made to cover the cost of this self-funded study. I am forever grateful to my parents and siblings, who have supported me throughout this journey. They made sure I persevered even when I was at my lowest point and thinking of quitting following the Covid pandemic and especially following my acid attack which knocked me to the ground. But by the will of the Lord all mighty and my parents, I strived ahead.

Finally, not forgetting my colleagues in the Surface Engineering Group that have become my friends and family at the university, thank you for all your support and the good time since the start of the journey.

Abstract

Fly ash, also known as pulverised fuel ash, is made from fine particles, spherical in shape, which vary in size, ranging from 0.5 to 2500 μm. Fly ash is a residue of coal combustion used in thermal energy generation; it is collected via a particle filtration method or using an electrostatic precipitator. Coal fly ash (CFA) consists of several elements including silicon, aluminium and iron. The toxicity level of CFA is dependent on the grade of coal used in the energy generation.

Electricity is mainly generated using coal as a source of energy in power plants, thus CFA is readily available in substantial quantities and this project has investigated routes to producing environmentally useful products from this waste material. Specifically, CFA has been coated with thin films of TiO_2 and Bi_2O_3 by means of the physical vapour deposition technique of magnetron sputtering. Thin films of TiO_2 and Bi_2O_3 have been known to be utilisied for antimicrobial uses, organic waste degradation and fluorine uptake. Thus, combining the coatings of TiO_2 and Bi_2O_3 would in return enhance the use of the CFA for multiple purposes including photocatalytic degradation, desalination, and defluorination. Coated CFA should be able to degrade organic compounds that have been disposed of in industry, like textile effluent containing dyes that have been used. Coated CFA may be used to help regulate fluoride levels in water treatment process.

Deposition of thin films of bismuth oxide and titanium oxide have been a research focal point, using two alternative magnetron sputtering set ups. Unbalanced magnetron sputtering is the method of choice, because of the high quality of the

coatings produced. Two set ups have been utilised in this research: a single target magnetron sputtering and a dual twin magnetron sputtering arrangement. Studying the results obtained from XPS, XRD and EDX analysis indicated that the TiO_2 and Bi_2O_3 coatings were successfully deposited on to the CFA particles. TiO_2 coated CFA, achieved by the dual twin magnetron sputtering arrangement, was deposited under a range of operating conditions. The best performing samples demonstrated strong results with dye degradation, achieving up to 89.1% decrease in absorbance. Other samples performed exceptionally well compared to TiO_2 bulk particles in absorbing fluorine at 32.20mg/kg and 35.59mg/kg, respectively.

The single target magnetron was utilised for the deposition of Bi_2O_3 onto the CFA, which demonstrated photocatalytic activity in dye degradation tests. The findings of the study shows that indeed coated CFA with either TiO_2 or Bi_2O_3 can be utilised for environmental purposes such as for dye degradation and defluorination.

Table Contents

List of equations,

List of Figures

List of tables

1.0 Introduction

1.1 Background

With the increase in electricity consumption in our day and age, power companies are under immense pressure to keep up with demand, as our lives depend on electricity. Putting numbers to the statement, in 1990, a total of approximately 10000 TWh of electricity was consumed, whereas, in 2021, total consumption surpassed 24000 TWh. Thus, electricity consumption (EIA, 2022) has more than doubled over the past two decades. Consumption will continue to increase with the shift towards the electrification of vehicles and homes to reduce dependency on gas, oil and coal. This leads to the questions of how our electricity is generated and what happens in the whole process, focusing on coal as a fuel source (Beretta, 2007).

For decades, coal-fired power plants have provided affordable, reliable, and constant power on demand to meet energy consumption needs. As much of the world lacks access to modern, clean energy, coal is still essential to meeting worldwide energy requirements, with approximately 40% of the world's electricity being generated utilising coal (Gohlke et al., 2011).

Countries within the European Union, along with America and the United Kingdom, have shifted away from relying mainly on coal as a source of fuel for generating electricity, though it is still in use. However, the rest of the world is still highly dependent on coal as the primary fuel source for generating electricity. However, there is an international emphasis on moving to cleaner energy to help with sustainability, global warming, and environmental pollution. With economic instability in different regions of the world, many nations with their own internal supplies, would rather depend on coal as the process is more accessible,

relatively cheaper, and easier to access than the high-end newer technologies applied for generating renewable electricity.

Later in the introduction of this thesis, we will explore in depth the adverse effects of relying heavily on coal as a fuel source and the methods currently in place to try and counteract the downsides of using coal.

Sustainability and environmental pollution have become a significant concern that needs to be addressed and is currently a major topic of discussion in the research world, intending to reduce waste products and increase recycling where possible to reduce the impact on the environment. The increase in pollution is directly correlated to the intoxication of all living creatures, humans, and animals alike.

The second line of motivation is waste treatment, mainly wastewater. Due to poor sanitation and water treatment around the globe and imminent freshwater shortages, an increasing number of people are forced to use water of a poor quality as a result of the high costs of water treatment. Developed regions such as the UK and EU have regulations to monitor the water being pumped back into the rivers and waterways. They are heavily monitored, but this is not the case in most countries worldwide. Many people rely on free-running streams and rivers as their primary water source for their daily usage, including washing, cooking, and drinking. People living near commercial plants are most impacted, along with living organisms in the water. This problem occurs in developing countries and the third world countries where regulations are not monitored or adhered to, they are responsible for approximately 80% of illnesses, including cholera, diarrhoea, Hep A, polio, and typhoid (Ashbolt, 2004; Manfredi et al., 2010).

Providing solutions will help improve the quality of the water being released, thus reflecting on the chance the locals accessing better quality of water. Furthermore,

it could enhance the water quality to levels deemed suitable for human consumption and not only for domestic use and agriculture (SME, 2021).

1.2 Aims and Objectives

This research aims to recycle one waste product, namely coal fly ash (CFA), to be utilised for environmental purposes such as water treatment, dye degradation and gas emission control to help reduce pollution in many forms it comes in. In simpler terms, it is an attempt to offer a novel solution to waste management with a secondary goal of addressing water quality issues and, potentially, air quality issues.

The following objectives have been the backbone of this research to achieve the aims:

Utilising CFA as a substrate for coating via the physical vapour deposition technique of unbalanced magnetron sputtering to achieve a photocatalytic film and exploring its use to degrade organic materials. The following key steps were undertaken:

1. Multiple analytical techniques were used to characterise and analyse the final coated materials, such as scanning electron microscopy (SEM), X-ray photoelectron spectroscopy (XPS), X-ray powder diffraction (XRD), and Raman spectroscopy to identify the materials phase, the external morphology, chemical composition and crystalline structure.

2. Different methods and experiments were used to determine the final product’s photocatalytic activity and usability for environmental purposes. The experiments include dye degradation tests, fluoride removal, desalination, and acetone degradation.

3. Optimising the efficiency of the coating process from the results gathered in the investigation stage to allow adjustments to be made for optimum activity.

The predominant aim of this research is to determine if the coating technique is compatible with the CFA substrate and is in fact a means by which CFA can be upcycled. However, the extent of this research's success will depend on whether these goals are met. it will pave the way for scaling up the approach to recycling a waste product that is abundant due to production, allowing for both environmental benefits and monetary gains. For example, generating revenue from coal ash sales, and cost savings from using coal ash in place of other, more expensive materials.

1.3 Novelty

The novelty of this research deals with several aspects:

In the first place, the coating process utilising a two-target magnetron rig, incorporating a specialised substrate holder made in-house to accommodate the coating of powders. The ability to manipulate the powders under two magnetrons in this manner has yet to be reported elsewhere (outside the Surface Engineering Group). In the process, the optimisation of the instrumental parameters for the coating process will be investigated. For this purpose, the well-known photocatalytic material titanium dioxide (TiO_2) will be employed, and the variations thereof as it is influenced by the coating process, characterised, and explored.

Secondly, a second coating process using a single target magnetron rig with an adapted substrate holder, also not reported elsewhere (outside the Surface engineering group), placed directly underneath the target. For this process, two materials have been employed titanium and bismuth.

Thirdly, while photocatalytic coatings of TiO_2 are nothing new, other materials combinations and singular materials with similar properties will be investigated. In this regard, coating fly ash with bismuth-doped titanium dioxide, will add another facet of novelty to this research.

Fourthly, utilising a single target magnetron rig to coat fly ash with bismuth oxide, and to determine photocatalytic permorformance under visible light has not been reported elsewhere.

In the final instance, a beneficiated waste material will be utilised to deliver an environmentally sustainable solution to typical pollution problems encountered in

wastewater treatment applications, water quality regulation and achieve fresh water.

1.4 Scope of investigation

This PhD will investigate the ability to coat fine spherical particles using a physical vapour deposition technique, magnetron sputtering, to ensure the quality of the coating formed. The coated particles undergo several tests to assess the quality of the coat and its performance.

The quality of the coating is determined by analytically characterising the coated sample using X-ray diffraction, X-ray fluorescence, Raman spectroscopy, scanning electron microscopy and X-ray photoelectric spectroscopy.

The performance of the coated sample is determined from the photocatalytic activity using different techniques, including dye degradation, desalination process and defluorination, which are described in detail later in this thesis.

1.5 What is covered

This thesis will cover the following sections and sub-sections,

- Section 2 Literature review covering wastewater pollution, fly ash, different types of surface coatings including chemical vapour deposition and physical vapour deposition, vacuum systems and achieving vacuum.
- Section 3 Methodology covering the detailed process of the coating process used in this research along with the analytical techniques and the testing experiments for photocatalytic dye and acetone degradation, desalination and defluorination
- Section 4 ties all the conducted experiments together discussing the materials used and the results from the experiments conducted.
- Section 5 is the summary of the research and conclusion noting further works to be carried out.

2.0Literature Review

2.1 Pollution

The nature of the pollution this research is aiming to tackle is predominantly fly ash landfill, which leads to other issues further discussed in depth at later stages of this thesis, along with water pollution and potentially air pollution.

2.2 Substrate in question

2.2.1 Coal fly ash explained

Coal, an organic sedimentary rock, mainly consists of carbon, along with oxygen, nitrogen, hydrogen, sulfur and various minerals (Ahamed et al., 2019). Coal is still used for generating electricity in many parts of the world, even with the push towards cleaner energy; more than 36% of the electricity generated relied on the use of coal in 2019 (Gottlieb et al., n.d.). According to the world coal association, 37% of today's electricity is from coal (*Coal & Electricity*, n.d.)

Coal is pulverised and combusted at temperatures ranging between 1200-1700°C in a furnace to boil water, generating high-pressure steam to turn the turbines (Ahmaruzzaman, 2010). Fly ash is produced as a waste by-product, collected in different means depending on the plant setup, including mechanical collectors, bag houses and electrostatic precipitators. The fly ash particles are generally grey, cenospheres in shape, varying in size ranging from 0.3 to 250μm (Li, 2014). Low in density 0.5±0.2g/cm^3 (Li et al., 2014; Bhatt et al., 2019)(Yu and Shen, 2015), they are usually amorphous and most likely alkaline. The composition of fly ash is predominantly metal oxides, which can be transition metals, and alkaline metals include aluminium oxide, magnesium oxide, silicon oxide (quartz) and calcium oxide. China reached 550 million tonnes of fly ash in

2018, India surpassed 200 million tonnes in 2020 in the United States of America generated over 120 million tonnes in 2016 in the production of CFA (Ding et al., 2017). The upside of using coal as a fuel is the simplicity of the process, which has been used for decades. The downside is the amount of fly ash and carbon dioxide produced due to the combustion of coal. There have been many efforts to recycle fly ash and reduce landfill and toxication to land and water.

CFA primarily consists of various metal oxides, as mentioned earlier, metal oxides, including aluminium oxide, magnesium oxide, silicon oxide and calcium oxide. The quality of CFA depends on the fly ash composition, and this brought about a classification system; the American Society for Testing and Materials (ASTMs) and the European standards explain that the percentage of SiO_2, Al_2O_3 and Fe_2O_3 are collectively used to determine the classification of the CFA. The classification may not hold any scientific merit (Visa et al., 2011; Dwivedi and Jain, 2014; Yao et al., 2015a). However, it has been adopted in the cement industry. Many argue that other vital factors, such as phase and mineral composition of CFA, for such classification to be scientifically recognised “Vassilev”. Vassilev states any elements that pose environmental concerns with a concentration of 50mg/kg should be included in the classification (Vassilev and Vassileva, 2007).

The coal grades adapted by ASTMs & ES are the ratio of oxides present that varies according to the quality of coal used and is primarily influenced by the region it was mined. Lower grade coal, sub-bituminous and lignite coals, have been found to contain higher percentages of MgO, CaO and SO_3 with lower percentages of Al_2O_3 and SiO_2. In contrast, higher-grade coal contains higher percentages of Al_2O_3 and SiO_2 and lower percentages of CaO, MgO and SO_3, be

it bituminous or anthracite. All types of coal are commonly used except for anthracite; only a few utility boilers use anthracite coal; hence only a little fly ash is generated (Ahmaruzzaman, 2010; Yao et al., 2015a; Jambhulkar et al., 2018). This classification, as you can see, isn't thorough enough, as mentioned by Vassilev, it doesn't cover the rest of the elements or a least, take into consideration toxic elements such as "arsenic" present in the CFA that contributes to global pollution (Vassilev and Vassileva, 2007). As mentioned above, millions of tons of fly ash are produced. However, only a portion of the CFA is recycled or reused. The most common application for CFA has been within the cement industry as an additive or a substitute (Gamage et al., n.d.; Iyer et al., 2001; Sugama et al., 2011; Nayak et al., 2022).

2.2.2 Hazards of fly ash

2.2.2.1 Environmental contamination: Fly ash can contain trace levels of heavy metals and other pollutants, such as mercury, arsenic, and lead; the amounts range from 8 to 139mg/kg, which can leach out of the material and contaminate the surrounding environment (Sushil and Batra, 2006). This can be a concern if the fly ash is used in construction materials that come into contact with water, such as concrete or bricks, or if it is stored in a manner that allows it to come into contact with water. In addition, fly ash may contain other contaminants that may harm human health, such as polycyclic aromatic hydrocarbons (PAHs).

2.2.2.2 Human health impacts: Some studies have suggested that exposure to fly ash may be associated with respiratory problems, such as asthma, and other

health problems, such as heart disease and cancer. These health risks are thought to be due to pollutants in fly ash, such as heavy metals and PAHs. However, the extent of these risks still needs to be fully understood, and more research is required to determine the potential health impacts of fly ash (Ahmaruzzaman, 2010; Yao et al., 2015b).

2.2.2.3 Disposal issues: Fly ash is typically stored in landfills or other waste management facilities. However, these facilities can be a source of environmental contamination if they are not correctly designed and managed. For example, if the fly ash is not adequately contained, it can leach into the surrounding soil and water, potentially contaminating these resources. In addition, the disposal of fly ash can be a source of greenhouse gas emissions, as the decomposition of organic matter in the fly ash can release methane, a potent greenhouse gas (Wang et al., 2020)(Verma et al., 2016).

2.2.2.4 Carbon emissions: **While using fly ash in construction materials can help reduce the overall carbon emissions associated with cement production, the production of coal fly ash is a source of greenhouse gas emissions. Coal burning to generate electricity releases carbon dioxide, a significant contributor to climate change. In addition, the transportation and disposal of fly ash can also cause greenhouse gas emissions. However, the net impact of fly ash on greenhouse gas emissions depends on various factors, including the efficiency of the power plant, the distance the fly ash must be transported, and the specific use of coal fly ash in construction materials (Hower et al., 2010; Sugama et al., 2011).**

Every year, vast amounts of coal fly ash are generated, which poses many issues, namely the disposing of such material. Fly ash is disposed of and stored in landfill sites; India uses 65,000m^2 of valuable land; the land used to keep this waste product could have been used for more beneficial and economic uses like agriculture (Jambhulkar et al., 2018). Moreover, fly ash's composition contains traces of toxic elements that may lead to environmental complications. This is especially so with the vast quantities being stored in landfill sites. Due to the small size of the fly ash particles, it can be assumed that they may become airborne and result in air pollution. Over time, they may cause skin and eye irritation and respiratory problems in humans and animals. In some extreme cases, it may cause arsenic poisoning. The storage of fly ash in a landfill may result in the fly ash particles being absorbed through the ground to sub-levels, causing heavy metal contamination of the groundwater. The rate at which the heavy metals and the toxic elements leach through the ground depends on a few conditions, namely the pH and solid/liquid ratio. Petra et al. investigated the leaching behaviour of the trace elements. They reported that the elements readily leached out from the stored fly ash, posing a threat to the air and surrounding land. After conducting tests on landfill sites, Neupane and Donahoe have suggested that landfill sites lined before the fly ash is deposited pose less of a risk of leaching compared to un-lined landfill sites (Dwivedi and Jain, 2014).

Depending on the coal being used, fly ash may contain traces of radioactive elements. When coal is in the whole state or in nature, such trace amounts do not pose a problem. They occur in trace amounts in nature, however, upon burning the coal. The trace elements, such as uranium and thorium, are concentrated tenfold from the original amounts (Jambhulkar et al., 2018).

Most of the parent coal's radioactive elements are distributed between solid combustion products and the gas phase.

The uranium from the coal fly ash sometimes leaches into the ground, consequently affecting the soil and water surrounding a coal plant, affecting cropland and, in turn, the food produced. People living within a "stack shadow"—within a half- to one-mile (0.8- to 1.6-kilometre) radius of a coal plant's smokestacks—might then ingest small amounts of radiation (McBride et al., 1978; Hvistendhal, 2007).

J. P. McBride at Oak Ridge National Laboratory (ORNL) and his associates examined the uranium and thorium levels of fly ash from coal-fired power stations in Tennessee and Alabama in a 1978 report for science. The scientists calculated the radiation exposure levels around the coal plants and compared them to exposure levels near boiling water reactors and pressurised-water nuclear power plants to determine precisely how damaging leaching might be (Hvistendhal, 2007)(McBride et al., 1978).

It was estimated radiation doses ingested by people in the vicinity of the coal plants were equal to or higher than the levels of people living around the nuclear facilities. The scientists' most extreme estimate of fly ash radiation in human bones was 18 millirems annually, in comparison to the population living around a nuclear plant showing radiation of 2 to 6 millirems annually (Hvistendhal, 2007).

Bhangare et al. tested six fly ash samples from different power stations that used different types of coal for combustion. They reported that all the samples were enriched with radioactive elements. Monitoring the type of coal used is crucial to reduce the possibility of radiation (Bhangare et al., 2014). Kovler investigated if the fly ash containing the radioactive elements posed a risk through its utilisation

in cement or road work. His findings illustrated that the radon exhalation rate was slightly high (Kovler, 2012). However, the radon emanation coefficients were low; the content of the radionuclides was within limits. The various reports concluded that the range of the radio nucleotides in the fly ash depends on the coal and the combustion condition, therefore, not posing a risk when used.

All these potential health and environmental risks will only worsen with the increase in coal consumption to meet energy usage and demand.

2.2.3 Current uses of fly ash

One of the primary uses of fly ash is as a supplementary cementitious material in concrete production. Concrete is a standard construction material used in many applications, including buildings, roads, bridges, and infrastructure projects. Concrete production is a significant contributor to greenhouse gas emissions due to the high energy demand and carbon dioxide emissions associated with the manufacture of Portland cement, a key ingredient in concrete.

Using fly ash in concrete can help reduce the overall carbon footprint of the material, as it can partially replace Portland cement. Fly ash can also improve the strength and other properties of concrete and its workability. Using fly ash in concrete can also reduce the demand for natural resources, such as limestone, used in cement production (Nayak et al., 2022).

In addition to its use in concrete, fly ash can also be used as a soil conditioner to improve soil's physical and chemical properties. It can reduce soil erosion and improve its ability to retain moisture and nutrients. This can be particularly beneficial in areas with degraded soil or where natural disasters, or human activities have damaged the soil (Iyer et al., 2001).

Fly ash can also be used as a filler in various construction materials, such as asphalt, brick, and plaster. The use of fly ash in these materials can help improve their strength and other properties and reduce their cost.

Overall, the use of fly ash in the industry can reduce greenhouse gas emissions, conserve natural resources, and improve the strength and other properties of construction, with its full potential not yet explored.

There have been a number of research papers published exploring CFA as a substrate to support photocatalytic material to be used for different purposes. They differ in the method of coatings.

Yu discusses how TiO_2 coated CFA by means of precipitation has shown positive results in nitric oxide NO with removal rates up to 67%. Yu has indicated that annealing temperatures effects the crystal size of anatase on the surface of CFA. The temperatures used vary between 300-700°C (Yu, 2004). Another research group reports the success of using CFA as a substrate for TiO_2 coating achieved with use of a single target magnetron sputtering system. A key feature that was mentioned is the substrate temperature of 350°C inorder to achieve an anatase phase of TiO_2. Following a deposition duration of 3 hours and tested for the degradation of methyl orange has shown remarkable results according to Yu (Yu and Shen, 2011). Shimizu et al, explored the use of CFA as a substrate and a dopent for TiO_2 coating used for waste water dye degradation. Utilising the sol gel coating technique the group succeeded in achieving the desired spherical geopolymer. Photocatalytic testing indicated a 48% decrease in the absorbance peak over a period of 8hours (Shimizu et al., 2020).

2.3 Surface coatings

Surface Engineering: a component interacts with the environment at its surface. This may be a mechanical interaction (e.g. friction, wear), a chemical interaction (e.g. corrosion), an interaction with light or other incident radiation (e.g. transmission or reflectance of light) or perhaps a biological interaction (e.g. antimicrobial or cell growth). Consequently, the surface's properties largely control the component's performance or ‘functionality’. Often, surface properties on the nanoscale can control performance on the macroscale. For example, 10nm thick silver films are used in architectural glazing products to limit heat loss through sheets of glass up to 6m x 3m in size (Saidur et al., 2008; Solovyev et al., 2015). Also, hard ceramic coatings of a few microns in thickness are used to prevent wear in steel cutting tools, allowing high-speed, lubricant-free machining operations to be carried out that would not be possible without the coating being present.

Surface engineering can be considered to be an enabling technology for advanced materials. Indeed, the importance of surfaces has led to the adoption of surface engineering technologies in most manufacturing sectors, including automotive, aerospace, digital technologies, consumer electronics, packaging, wearable tech, healthcare, built environment, energy and biomaterials. Surface engineering allows the modification or coating of a component or substrate surface to provide specific functionality or functionalities to the component. In cases as diverse as jet turbines and mobile phone displays, the coating is ‘mission critical’, and the component couldn’t function effectively without it. The discipline includes many competing technologies, ranging from well-established

techniques, such as electroplating or thermal spraying through, to emerging nanoscale technologies, such as atomic layer deposition and molecular beam epitaxy. The Surface Engineering Group at Manchester Metropolitan University mainly specialise in a physical vapour deposition technique, referred to as magnetron sputtering, which finds widespread use in industry.

The most recent findings, reported by the Surface Engineering and Advanced Coatings Special Interest Group (SEAC) in 2014, are that the UK surface coatings industry has a turnover of about £11 billion, the products critically affected by coatings have a value of over £140 billion, and these are used in industrial sectors which together have a turnover value in excess of £383 billion to the UK economy each year.

Many different techniques can be utilised to coat desired materials on to the substrate in question. The ultimate goal is to modify the surface to become useful by introducing different layers by different means, which in turn alters the behaviour of the substrate deeming them useful for a given purpose. Thin film coatings can result in altering the structure, morphology, composition, and life expectancy of the material. Vapour phase coating process can be defined by two major categories: chemical and physical vapour deposition. Each method has its own merits; the choice of technique is dependant of the resources available and the desired coating. There are a few points to keep in mind when making the choice of coating method, such as the application of the thin film and the characteristics of the coated component. This chapter will discuss different methods of coating used in industry and the method of choice of this research, magnetron sputtering.

2.3.1 Chemical vapour deposition; CVD

Chemical vapour deposition (CVD) is a process used to deposit thin films of material onto the substrate using a chemical reaction between gas(es) or vapour and the surface of the substrate. In CVD a gas or vapor carrying the desired material is introduced to a reactor, where it is exposed to a substrate that is heated to a high temperature ranging between 800 to 1000°C (Carlsson and Martin, 2009; Fuentes, 2010). The high temperature causes a chemical reaction between the gas or vapor and the surface of the substrate, resulting in the deposition of a thin coating films ranging from 0.5 – 2000 μm that are a well-adhered and uniform, and dense coating of the desired material onto the substrate (Sawtell et al., 2009; Sawtell, 2011).

CVD is widely used in a variety of applications, including the production of coatings, thin films, and electronic devices. It is particularly useful for producing thin films with good electrical and optical properties, as well as for producing coatings with good corrosion and wear resistance. There are several advantages to the CVD process. A couple of benefits is its ability to produce thin films on different shaped substrate include tubular shaped substrates with good control over the thickness and composition of the film, allowing for precise tailoring of the film's properties to meet the application's specific needs.

In addition, CVD is a relatively fast and efficient process, as it allows for the simultaneous coating of multiple parts or items. It is also capable of depositing a wide range of materials, including metals, alloys, and ceramics, allowing for a high level of versatility in the types of products that can be produced (Sawtell et al., 2009; Sawtell, 2011).

However, there are also some drawbacks to the CVD process. One of the main challenges is the process generates hazardous waste materials, which must be properly managed and disposed of to prevent environmental contamination.

Overall, CVD is a useful coating technique with a wide range of applications in producing coatings, thin films, and electronic devices. It allows for the precise control of the film properties and can deposit a wide range of materials; it can prove to be potentially a hazardous process. Chemical vapour deposition (CVD) is used to produce high-quality thin films, which are often used in the semiconductor industry due to the technique's low cost. The desired coating is achieved when the precursors in the vapour phase react and adsorb onto the substrates' hot surface. However, when using the CVD method, one is challenged with the formation of hazardous by-product gasses, for example, HCL gas, from the reaction that must be released from the system safely.

[Eq.1] $TiCl_4 + H_2O \rightarrow TiO_2 + HCl$

The above [Eq.1] is a shortened example of the reaction that takes place in order to achieve TiO_2 coatings on the substrate, while releasing HCl gas (Wasa et al., 2004; Torres-Huerta et al., 2016; Li et al., 2019).

2.3.1.1 Electroplating

Electroplating is a coating technique that involves applying thin layers of metal onto the surface of a substrate using an electrochemical process. The metal is dissolved in a solution and is applied to the substrate by passing an electric current through the solution. As the current flows, the metal ions are attracted to the substrate, and deposited in a thin, uniform layer (Ojo and Dharmadasa, 2018).

Electroplating is used in various applications, including producing decorative items, such as jewellery and home decor, and functional items, such as automotive parts and electronics. It is also used in making printed circuit boards and other electronic components, as it allows for the precise application of metal layers to create complex circuits.

There are several advantages to the electroplating process. One of the main benefits is that it allows for the precise control of the thickness and uniformity of the metal layer. Electroplating is particularly important in producing electronic components such as chips, where the accurate thickness and uniformity of the metal layers are critical to the device's performance to prevent heat resistance and allow for electrical conductivity.

Electroplating is also a relatively fast and efficient process, as it allows for the simultaneous coating of multiple parts or items. This makes it well-suited for mass-production applications. In addition, electroplating can be used to apply a wide range of metals, including gold, copper, brass, and nickel, allowing for a high level of versatility in the types of products that can be produced (Ojo and Dharmadasa, 2018; Mersagh Dezfuli and Sabzi, 2019).

There are potential drawbacks to the electroplating process. One of the main challenges is the disposal of waste products that are generated during the process. Electroplating generates hazardous waste materials, including heavy metals and other pollutants, which must be appropriately managed and disposed of to prevent environmental contamination. In addition, the process requires using hazardous chemicals, which can harm workers if not properly handled (Andricacos et al., 1908; Giurlani et al., 2018; Rajoria et al., 2022).

Overall, electroplating is a widely used coating technique with many benefits, including precise control of the metal layer, high efficiency and versatility, and the ability to apply a wide range of metals.

2.3.1.2 Sol-gel coating

The sol-gel method of coating became very popular in the 1900s for ceramic coatings on a large scale due to it being a simple process that generally entails three steps: hydrolysis, condensation and drying and the ability to fabricate metal oxides. The process involves:

- The Sol is a solution of colloids (particles 1-100nm in size) in which the substrate is submerged.
- Allowing the particles to react and condense.
- Changing state into a gel - a porous interconnected network of particles on the substrate.

The newly formed gel is then dried to produce the desired ceramic/glass coating of a porous nature.

Sol-gel coatings have several attractive properties, including good chemical resistance, high hardness and wear resistance, and excellent corrosion resistance. These properties make sol-gel coatings well-suited for various applications, including protecting metal and other surfaces against corrosion and wear (Hench and West, 1990; Thoř and Václavík, 2016; Dehghanghadikolaei et al., 2018).

One of the main advantages of sol-gel coatings is their ability to produce thin, uniform layers of material with good control over the thickness and composition of the coating. This allows for the precise tailoring of the properties of the coating to meet the specific needs of the application (Dehghanghadikolaei et al., 2018).

Sol-gel coatings can be applied using various methods, including dip coating, spin coating, and spray coating. These methods allow for the efficient and cost-effective production of sol-gel coatings on various substrate materials, including metals, ceramics, and polymers.

Sol-gel coatings have been used in many applications, including anti reflective coatings, batteries and electrical devices such as capacitors and sensors. Along with environmental application with likes of catalysts and adsorbent materials. They have also been used in producing optical coatings, such as those used in lenses and mirrors, and in producing protective coatings for solar cells (Yu et al., 2016).

2.3.1.3 Wetness impregnation

Wetness impregnation is a process that involves the application of a liquid or aqueous solution to a solid material to alter its properties or to introduce a desired component into the material. Wetness impregnation is commonly used in a variety of applications, including the manufacture of coatings, adhesives, and composite materials.

One of the main advantages of wetness impregnation is that it allows for the coating of materials that poses complex geometries and irregular surfaces. This can be particularly useful in the production of coatings and adhesives, where the uniformity and thickness of the applied material are critical to the final product's performance (Deraz, n.d.; Mehrabadi et al., 2017).

Wetness impregnation can be carried out using various methods, including dipping, spraying, and roll coating. These methods allow for the efficient and cost-effective application of the impregnating material to the substrate.

In the production of coatings and adhesives, wetness impregnation is often used to introduce functional components, such as pigments, fillers, and curing agents, into the substrate. These components can be used to improve the final product's performance, such as by increasing its strength, durability, or resistance to environmental factors.

Wetness impregnation is also commonly used in the production of composite materials, where it is used to introduce reinforcement fibres or particles into a matrix material. These reinforcement materials can improve the composite material's mechanical properties, such as its strength, stiffness, and toughness.

Overall, wetness impregnation is a useful process that allows for the introduction of desired components into solid materials, potentially improving the final product's performance and functional properties.

2.3.2 Physical vapour deposition PVD

Physical vapor deposition (PVD) is a family of coating techniques that include sputtering, evaporation, ion plating and electron beam evaporation. The basis of PVD involves the application of a thin layer of material onto a substrate using a process that involves the physical vaporisation of the coating material from a solid source under a partial vacuum. In PVD, the coating material is typically vaporized by heating it to a high temperature or by bombarding it with high-energy particles, such as ions. The vaporized material is then deposited onto the substrate in a thin, uniform layer (Seshan, 2002).

PVD is used in a variety of applications, including the production of decorative coatings, functional coatings, and protective coatings. Decorative PVD coatings

are used to impart a desired appearance to a product, such as a metallic finish or a coloured finish. Functional PVD coatings are used to improve the performance of a product, such as by increasing its wear resistance, corrosion resistance, or electrical conductivity. Protective PVD coatings are used to protect the surface of a product from environmental factors, such as wear, corrosion, and heat (Donald M Mattox, 2010; Matthews, 2013).

There are several advantages to the PVD process. One of the main benefits is that it allows for the precise control of the thickness and uniformity of the coating. PVD coatings can be applied to a wide range of substrate materials, including metals, ceramics, and polymers, and can be applied to complex shapes and geometries. PVD coatings typically have dense structures making them relatively hard and durable and can provide excellent corrosion and wear resistance.
There are also some potential drawbacks to the PVD process. One of the main challenges is the high capital and operating costs associated with the vacuum equipment and materials used in the process. In addition, PVD coatings may be sensitive to certain environmental factors, such as temperature and humidity, which can affect their performance.

Overall, PVD is a useful coating technique that has a wide range of applications in the production of decorative, functional, and protective coatings. It allows for the precise control of the coating properties and can provide excellent corrosion and wear resistance to the coated product (Inspektor and Salvador, 2014).

2.4 Magnetron Sputtering

Sputtering is a process used to deposit thin films of material onto a substrate by vaporising the target material (or cathode) using energetic particles, usually ions, impacting the target (Kelly and Arnell, 2000). Sputtering relies on generating a plasma, or ionised gas positioned in front of the target; the bombardment process "vaporises" the target material. The vaporised material is sputter "deposited" onto the substrate in a thin, uniform layer. Along with sputtered atoms, secondary electrons emitted are used to maintain the plasma. This technique has been around for around 150 years and has been successfully used to deposit desired materials. The downsides to the sputtering process are the inefficiency of ionisations, deposition rate, and high substrate heating (Kelly and Arnell, 2000). To overcome the hurdles and limitations magnetron sputtering has been developed. Magnetron sputtering is a high-power device, simultaneously a high-frequency device if a pulsed power source was utilised. Magnetron sputtering relies on magnets to restrict the movement of secondary electrons to the target area. Therefore, it increases the chance of ionising collisions of the electrons with background gas atoms, which in turn increases target bombardment, increasing the deposition rate (Ratova, 2013).

Furthermore, increased ionisation allows for lower operating parameters, pressure and voltage than basic sputtering (pressures 10^{-3} mbar compared to 10^{-2}mbar and -500V compared to -2/3kV). There are two types of magnetron sputtering, balanced and unbalanced, and they are largely similar with a slight difference in design. They are described in more detail further down in this chapter.

Magnetron sputtering is utilised in a variety of applications, including the production of coatings, thin films, and electronic devices. It is beneficial for producing coatings with good adhesion, wear resistance, and corrosion resistance and for making thin films with good electrical and optical properties (Donald M. Mattox, 2010).

Several different types of magnetron sputtering power source**s**. include DC magnetron sputtering, mid frequency pulsed DC, RF magnetron sputtering, and hybrid magnetron sputtering may be used.

DC magnetron sputtering is the most common type of magnetron sputtering, and it is used to deposit a wide range of materials, including metals, alloys, and ceramics. In DC magnetron sputtering, a direct current is applied to the magnetron, and the ionisation of the gas generates the plasma in the vacuum chamber. DC magnetron sputtering is a relatively simple and low-cost process with restrictions to the materials that can be deposited and the thicknesses of the coatings that can be achieved. DC magnetron sputtering may not be used in the deposition of insulating materials as the electron flow may not pass through (Kelly and Arnell, 2000; Musil et al., 2005; Donald M. Mattox, 2010).

RF magnetron sputtering is a variation of magnetron sputtering that uses radio frequency typically 13.56MHz power to generate the plasma. RF magnetron sputtering is more flexible than dc magnetron sputtering, as it allows for the deposition of a broader range of materials including insulating material and achieves thicker films. However, it is also a more complex and expensive process (Donald M. Mattox, 2010)(Ratova, 2013).

Hybrid magnetron sputtering is a combination of dc and RF magnetron sputtering, and it combines the advantages of both techniques. Hybrid magnetron sputtering

allows for the deposition of a wide range of materials and the achievement of thick films while maintaining the simplicity and low cost of DC magnetron sputtering (de Castilho et al., 2022).

Balanced magnetron sputtering and unbalanced magnetron sputtering are two variations of the magnetron sputtering process apart from the power source described above.

In balanced magnetron sputtering, the plasma is generated by the ionisation of the gas in the vacuum chamber, different power supplies may be applied and the balanced magnetron has a magnetic field that is balanced, or symmetrical, around the magnetron. This results in low ion currents to the substrate and result in lower quality films. However, unbalanced magnetron sputtering may be used in specific applications where a less consistent film is desired or where the cost or complexity of a balanced magnetron sputtering system needs to be justified (Donald M. Mattox, 2010).

Unbalanced magnetron sputtering is similar to the balanced magnetron sputtering. However, the magnets are arranged differently, in which the outer magnets are strengthened. The unbalanced magnetron arrangement allows for the secondary electrons to follow the magnetic field lines towards the substrate. Therefore, allowing the extraction of high ion current from the plasma without having to externally bias the substrate. But the current applied to the magnetron is not balanced around the magnetron. As a result, the magnetic field generated

by the magnetron is asymmetrical. A schematic diagram of the magnetic arrangements is shown below (Kelly and Arnell, 2000).

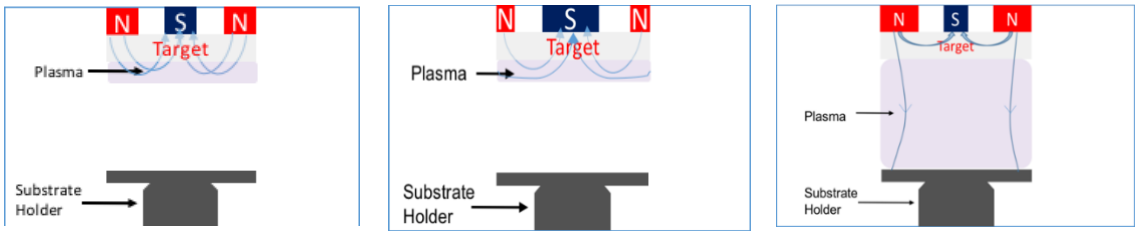

Figure 5: A schematic diagram of the plasma confinement in the balanced and unbalanced magnetron sputtering.

With unbalanced magnetron sputtering, the deposition rate is directly proportional to the target current. Increasing current and, by default, increasing the deposition rate does not affect the ion-to-atom arrival ratio at the substrate (Kelly and Arnell, 2000). As illustrated in the schematic diagram above, there are two types of unbalanced magnetron sputtering: type 1 unbalanced – the centre pole is stronger than the outer poles and type 2 unbalanced – the outer poles are stronger than the centre poles.

Reactive magnetron sputtering is a form of a PVD technique that depends on ion bombardment in the presence of a gas, such as oxygen, to achieve highly reproducible oxide and nitride coatings with minimal variance (Donald M. Mattox, 2010).

As stated earlier, reactive sputtering depends on introducing another gas to a system under a vacuum in the presence of an inert gas, such as argon. As stated earlier it is used in the deposition of coatings and films be it dielectric or insulating such as oxides. Metal targets are preferred due to the higher deposition rate compared to dielectric targets and are easier to maintain the discharge. The

process requires coating to be precise; hence the reactive gasses introduced into the system must be monitored and controlled; this is achieved with the aid of flow controllers produced by MKS instruments. Without maintaining the correct flow of the gasses, we risk "poisoning" the targets; this refers to a ceramic layer forming on the surface of the target, insulating it from successfully reacting with O_2. A high reactive gas flow and low deposition rates can determine this. It is crucial to have the proper flow of the reactive gas, oxygen, to maintain "metallic mode" high deposition rate with low reactive gas partial pressure. While simultaneously avoiding "poisoned mode" with a low deposition rate and high partial pressure (Ratova, 2013; Ratova et al., 2017).

Sputtering works by ions striking the target of the desired material with sufficient energy to remove atoms of the target material in a momentum exchange mechanism. The sputtered particles are then free to move within the vacuum chamber, whereas the charged particles are directed by the magnetic field to adsorb and react on a substrate (Kelly and Arnell, 2000).

In order to accomplish the process of sputtering, several steps must be taken. Firstly, the deposition chamber must be evacuated of air to create a vacuum.The process by which vacuum is achieved is described in section 2.5.1. Creating a vacuum reduces unwanted impurities within the film and increases the ejected particles' mean free path, increasing the probability of them reaching the substrate and embedding. A magnetron setup is illustrated in section 3.2.1.1.

As mentioned earlier, magnetron sputtering is the method of choice for coating. Using a DC power source can result in charge build up on the cathode deeming the target surface “poisoned” which results in “arcing” ". A pulsed DC power supply prevents arcing and allows for a higher deposition rate than RF sputtering.

Preventing charge build-up on the poisoned target precludes the occurrence of the arcing, made possible by limiting the pulse-on period. During the downtime of the pulse period, "pulse-off", the charge is dispersed through the plasma as the target voltage becomes more positive—correct parameters, such as cycle duty and pulse frequency, aid arc-free deposition (Kelly and Arnell, 2000; Donald M Mattox, 2010; Ratova, 2013).

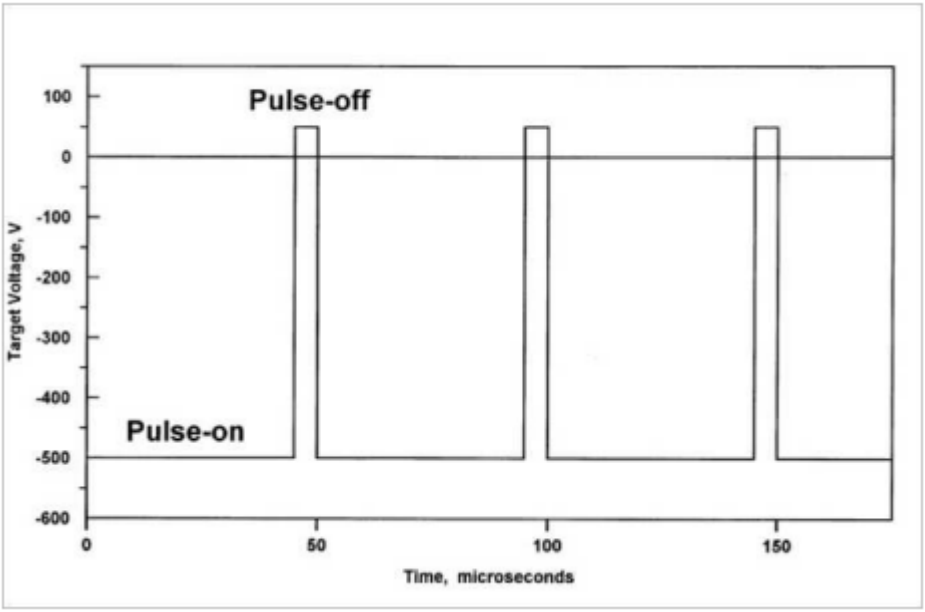

Figure 6: Schematic representation of target voltage waveform for a pulsed DC power supply.

The frequency used during pulsed DC sputtering ranges between 50-350kHz, limiting the pulse-on period, resulting in charging and arcing being unable to occur in the poisoned regions of the target (Ratova, 2013).

2.5 Vacuum

A space barren of matter, where the pressure in a specific system is lower than the atmospheric pressure, is called a vacuum. There are a wide variety of uses for vacuum techniques in the industrial sector; some of the more well-known applications of vacuum processes are as follows:

•Removal of water by the process of evaporation from the frozen state. In the food business, along with pharmaceutical and biological industries, it is used for temperature-sensitive functions, known as freeze drying.

• The semiconductor industry requires a controlled vacuum environment to manufacture silicon chips in the precise configuration required.

• Vacuum leak testing is utilised in various industries, including the electronic industry, aircraft, and atomic energy. A vacuum mass spectrometer is one of the accurate methods for locating gas leaks and even liquid leak.

• Vacuum coatings allow for the execution of different deposition processes thanks to a high vacuum. The coatings deposited by vacuum procedures have applications in various industries, including those that deal with construction materials, optical coatings, wear-resistant and hard coatings, and so on.

Vacuum can be categorised into ranges that depends on the absolute pressure.

- Atmospheric pressure: 1×10^{5} Pa
- Low vacuum: 1×10^{5} – 1×10^{3} Pa
- Medium vacuum: 1×10^{3} – 1×10^{-1} Pa
- High vacuum: 1×10^{-1} – 1×10^{-7} Pa
- Ultra-high vacuum: 1×10^{-7} – 1×10^{-10} Pa

2.5.1 Achieving vacuum in the system

The process of creating a vacuum begins with atmospheric pressure in the chamber. With a vacuum pump connected to the chamber pumps gas molecules out of the chamber, resulting in a vacuum. The gas molecules are in a viscous flow regime at the start of a pump down. Frequent frictional interactions distinguish this flow between molecules. When some molecules are removed, the number within the given volume immediately equalises. Removing molecules in a viscous flow regime can be accomplished using a rotary pump which is positive displacement pump. Achieving molecular population equilibrium takes longer as more molecules are removed from the chamber, and fewer molecules are removed in each pump cycle as more molecules are removed. Molecular flow refers to the state in which molecules have no frictional interactions. Here, the only factor controlling the flow from the chamber to the pump is the possibility that a molecule will diffuse into the pump at any given time. Using a high vacuum pump, such as a cryopump, turbomolecular, or vapour diffusion, additional gas molecules can be removed from the chamber. Another critical aspect of the vacuum process is the selection of the appropriate pump (Rao et al., 1961).

Because no single pump can reach the vacuum pressure required, a sequence of pumps are usually employed to create a high vacuum. Pumps are classified into two types: high vacuum pumps and to create low vacuum, roughing pumps are used.

Figure 1 is a schematic illustration of the rotary pump with a rotary vane, one of the most common types of roughing pumps. This pump employs rotational motion to reduce volume, thereby increasing trapped gas pressure.

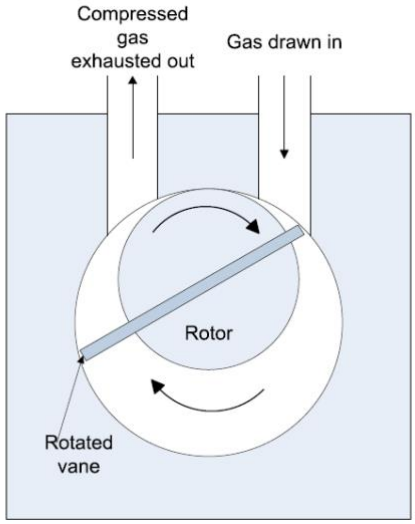

Figure 1: depicts a schematic overview of a rotary pump (Ratova, 2013).

The rotary pump is a positive displacement pump that uses a device to expand a space repeatedly, admit gases to flow into the space, block off the cavity, and discharge it into the atmosphere. Two-stage rotary pumps have two chambers, with the exhaust of one chamber increasing in pressure by passing through the second compression stage (Bishop, 2007).

The diffusion pump Figure 2 is a form of momentum transfer pump that expels gas molecules from a chamber using high-speed jets of dense fluid or high-speed spinning blades. A diffusion pump works by vaporising a liquid (usually oil).

The vapour is guided towards the core of the pump and down towards the cooled pump body. When the vapour from the jets interacts with the existing gas in the pump and directed to the lower parts of the pump. The condensed vapour drains to the reservoir at bottom due to the cooled pump surfaces, and then reevaporates. Therefore, the pressure increases at the bottom of the pump and decreases at the top.

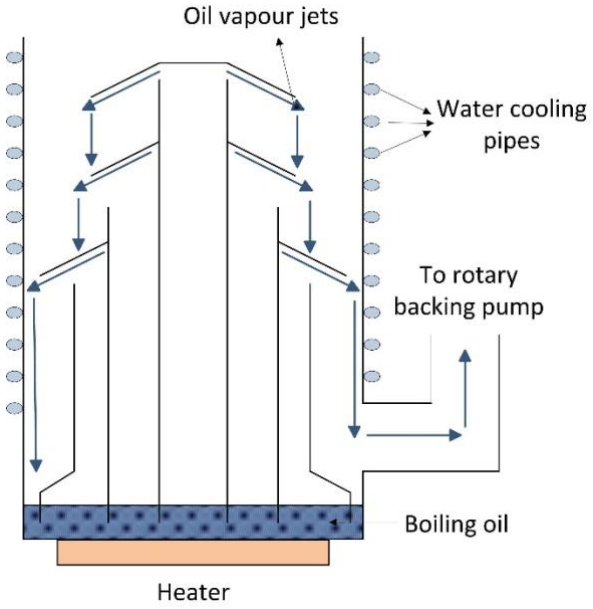

Figure 2: depicts an overview of the diffusion pump (Bishop, 2007)

Diffusion pumps achieve high vacuum, which can be as low as 10^{-8} Pa, depending on the vacuum system configuration. The primary advantages of diffusion pumps over other types of high vacuum pumps are their high pumping speed and low cost per unit of pumping speed. Diffusion pumps are durable, with no moving parts, and are simple to upkeep and fix. The danger of oil back streaming into the vacuum chamber and polluting the coatings is one of the most significant disadvantages of diffusion pumps. Because the diffusion pump cannot be subjected to the atmosphere because it will oxidise the oil. the mechanical roughing pump should be used to reduce pressure at the beginning of the pumping cycle. To achieve high vacuum, turbomolecular pump or a cryopump could be used as an alternative to the diffusion pump (Ratova, 2013).

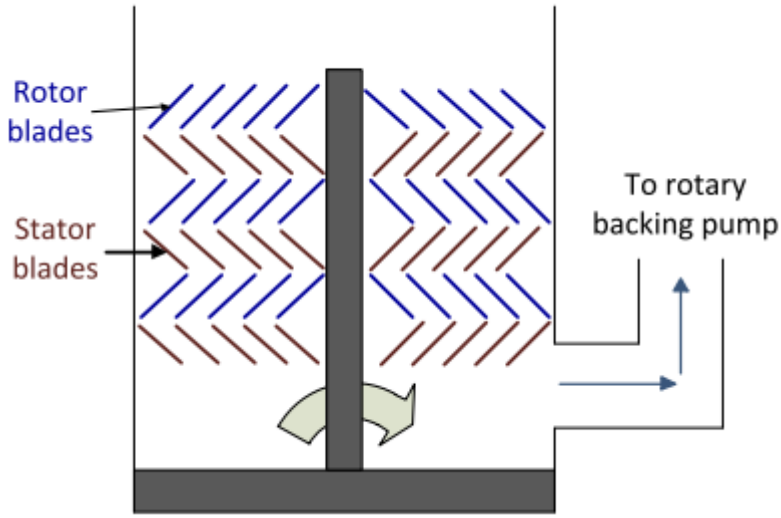

Figure 3: The turbomolecular pump is depicted schematically (Ratova, 2013).

The turbomolecular pump, like the diffusion pump, is a high vacuum pump that belongs to the momentum transfer pump family. It comprises a high-speed shaft and a series of multibladed rotor/stator pairs. Rotors and stators with angled blades capture the gas at the upper stages and force it down to the lower stages. When the gas molecules reach the lowest stage of the pump, they are moved out

through the exhaust, which is usually piped out to the roughing line. The turbomolecular pump can achieve high vacuum down to 10^{-8} Pa. However, it is far more effective in pumping heavy molecules than lighter ones since the compression ratio varies exponentially with the square root of the molecular weight of the gas (Harris, 1989; Bishop, 2007). One advantage of a turbomolecular pump over a diffusion pump is that it does not introduce oil vapour into the vacuum chamber thus preventing contamination (Ratova, 2013). the turbomolecular pump typically employs magnetic bearings to ease friction, to avoid the use of oil. The disadvantage of turbomolecular pumps is the high cost associated with the high grade of bearing necessary due to the high rotor speed.

2.5.2 Monitoring the vacuum in the system

2.5.2.1 PIRANI

Pirani gauges are a type of vacuum gauge utilised to measure the pressure of gases within a system under a vacuum. Guido Pirani, who designed the first Pirani gauge in the 1920s, is recognised as the one who gave these gauges their names.

The basic premise upon which Pirani gauges works is that the thermal conductivity in response to variations in the pressure of the gas that surrounds the wire. A Pirani gauge works by employing an electric current to raise the temperature of a wire to an extremely high level. Following this step, the wire is made to come into contact with the gas contained within the vacuum system. The pressure of the gas is then determined by observing the variations in the wire's electrical resistance.

In a wide variety of vacuum systems, such as those used in scientific research, industrial processes, and manufacturing, Pirani gauges are frequently put to use to measure the pressure of the gases contained within those systems. They are beneficial in high-vacuum applications, in which other kinds of gauges would not be able to function effectively.

Pirani gauges measures thermal conductivity in environments with low levels of vacuum: Atm Pressure to 0.1Pa (Bishop, 2007). When heated, the gauge, constructed out of a metal filament, lose heat upon interaction with the gas molecules. The more molecules collide with the filaments, the more heat is scattered, and the pressure builds. Similarly, the pressure of the filament will increase in tandem with the temperature. The relationship between the electrical resistance of the filament and its temperature is measured using a Pirani gauge. This is possible because the heated filament is a component of the bridge circuit. Following that, the value of the resistance can be translated into pressure values (Bishop, 2007).

This sort of gauge is sensitive to the kind of gas that is being used, which results in varied amounts of heat being withdrawn from the filament. This is because the masses of various gases can vary significantly from one another. As a consequence of this, the Pirani gauge needs to be adjusted so that it is accurate for the gas that will be used. The range of pressures that may be accurately measured using Pirani gauges is from 0.13 to 133 Pa (Harris, 1989; Bishop, 2007).

Pirani gauges offer a number of benefits, the most notable of which are their affordability, ease of use, and dependability. In addition to this, it is straightforward to calibrate and maintain them. However, their precision is susceptible to being affected by variations in temperature, and they are less accurate than some other types of vacuum gauges.

2.5.2.2 Penning Gauge

Another means of measuring the pressure in the chamber is the Penning gauge. The Penning gauge makes use of the current that is generated by a glow discharge. The glow discharge is brought about by an applied voltage of around 2 kV. The pressure level can be determined by measuring the produced electron and ion currents. This type of gauge can have a variety of different geometries. Still, it is typically made up of an anode in the middle, a cylindrical cathode around it, and a concentric magnet with both (Ratova, 2013). Figure 4 illustrates the Penning gauge's overall schematic layout. The use of the Penning gauge is subject to certain restrictions. If the pressure is too high, it is impossible to produce a glow discharge because there will be an excessive number of molecular collisions, which will lead to the loss of energy. When the pressure is too low, a glow discharge cannot be formed because there are not enough collisions to keep the glow discharge going. This prevents the glow discharge from occurring. The penning gauge has a pressure range of 1.3 Pa to 1.3 mPa.

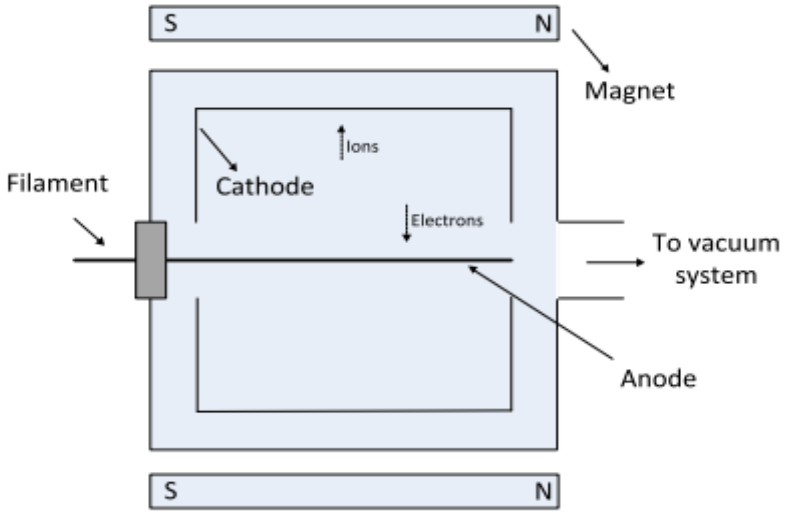

Figure 4: Penning Gauge schematic diagram (Ratova, 2013)

2.5.2.3 Baratron - Capacitance manometer

A transducer that converts a pressure input into an electrical output signal is called a Capacitance manometer. The applied pressure is proportional to the output signal, which can be used to display or regulate the pressure. Baratrons are commonly employed in high-precision pressure measuring applications because of their stability and long-term accuracy (Sullivan, 1985).

A Baratron operates on the variable capacitance principle. A device's capacitance varies in proportion to the amount of pressure applied. The pressure to be measured is applied to a diaphragm coupled to a capacitor in a Baratron. The diaphragm moves as the pressure varies, changing the capacitance of the capacitor. The change in capacitance is then translated into an electrical signal proportionate to the pressure, usually a voltage in the range 0-15V (Bishop, 2007).

Baratrons come in various pressure ranges, ranging from low-pressure vacuum measurements to high-pressure measurements. They're frequently found in a vacuum, process control, and test and measurement equipment. Baratrons can be used to monitor both vacuum and pressure, and they can measure pressures as low as 1Pa and upto 20kPa (Ratova, 2013).

Baratrons are highly accurate and steady, with an accuracy of less than 0.1% of full-scale. They are also relatively resistant to temperature change, due to the internal heaters the aid with maintaining a constant temperature and vibration, making them ideal for usage in severe locations.

Baratrons are high-accuracy pressure transducers that employ the variable capacitance principle to transform pressure into an electrical output signal. They are well-known for their stability and accuracy in vacuum and pressure-measuring applications. They are available in various pressure ranges and can be used to measure both vacuum and pressure (Sullivan, 1985; Higham and Paros, 2010).

2.6 Materials deposited by magnetron sputtering on CFA.

2.6.1 Titanium Dioxide

Titanium dioxide (TiO_2) is achieved from a reaction between titanium and oxygen. Titanium dioxide occurs in nature in the form of the mineral's rutile and anatase. Titanium dioxide has many applications, due to is properties namely: chemical stability, physical, optical properties and it is low cost and high oxidizing power. The journey of titanium dioxide began as a non-toxic replacement for lead oxide as a pigment in a white paint. As a pigment TiO_2 has been used in different industries including pharmaceuticals cosmetics and food manufacturing. The ability of TiO_2 to lower the incidence of Sun's rays make it suitable for sunscreens and UV blockers on thin films (Oi et al., 2016). Furthermore, TiO_2 is utilised in ceramic glazes to maintain colour and to combat yellowing of the surface.

Titanium dioxides photocatalytic properties were first discovered in Japan circa 1967 by Fujishima and published in 1972 (FUJISHIMA and HONDA, 1972). Since the discovery a lot of research has been deployed into its photocatalytic properties. Titanium dioxide being a semiconductor has a band gap of 3.2eV to be photocatalytic active (Bagheri et al., 2014). In order to be activated; UV rays (wavelength less than 385nm) are absorbed causing an electron to move from the valence band to the conduction band generating electron hole pairs instigating the photocatalysis Process (oxidation and reduction reaction) as depicted in [Eq.2] (Pelizzetti and Minero, 1993).

$$[\text{Eq.2}]\ TiO_2 + e^- (>3.2eV) \rightarrow h^+ + e^-$$

The photocatalytic properties of TiO_2 grants it use in different applications including self-cleaning surfaces, air purification and water treatment. The electron hole pairs generated from the interaction between the UV rays and TiO_2 are paramount in the process of the breakdown of the organic pollutants and bacteria. The reaction does not produce any by-product as the organic pollutants are degraded to non-toxic substances (Pelizzetti and Minero, 1993).

There are 2 phases of TiO_2 that predominantly exhibit photocatalytic activity. Anatase and Rutile phases can be achieved from altering the crystal phase by means of annealing. Anatase has a tetragonal structure whereas rutile exhibits a tetrahedral structure. The bandgap values differ from 3.2eV and 3.0eV for anatase and rutile respectively. Even though rutile has a lower bandgap value anatase exhibits better photocatalytic properties. It is suggested that the fermi level is responsible for increase in the photocatalytic activity. Higher fermi level in anatase is responsible for higher levels of level of hydroxyl groups on the surface. Furthermore, the indirect band gap in anatase results in the ability of electrons to stabilise at lower conduction bands, hence, results in greater charge carrier mobility and a longevity (Luttrell et al., 2014).

In this research a standard was used for comparison, the commercial available titania PC500 provided by CristalACTiV™, dedicated to photocatalytic applications that posses high surface area with an ultra high purity.

2.6.2 Bismuth Oxide

Bismuth oxide Bi_2O_3 has been investigated more in recent times, being a semiconductor with properties that promote its use in different fields. Bi_2O_3 possess a wide band gap (2.6eV) and refractive index which allow for it to be a good photocatalyst and a photoanode. Bi_2O_3 also possess photoconductive and photoluminescent properties (Kumari et al., 2007). These properties allow Bi_2O_3 to be utilised in solid support catalyst, sensor, solid oxide fuel cells, lithium batteries and fire-retardant materials (Jagdale et al., 2017)(Kumari et al., 2007).

There are several structures (phases) that Bi_2O_3 can form, the meta stable phase: -tetragonal -bodycentred cubic are of predominant interest due to their photocatalytic properties for environmental remediation under visible light (Ratova et al., 2018).

A few research papers have been published discussing the use of fly ash as a binder with Bi_2O_3 in the construction industry to make self-cleaning coating on concrete as described by Luevano-Hipolito (Luévano-Hipólito et al., 2019). However, there ae no records of papers discussing coating fly ash with Bi_2O_3. Ratova discusses the efficiency of bismuth oxide coatings on glass beads and antimicrobial performance under visible light. It was found the photocatalytic performance of Bi_2O_3 where better than other known photocatalyst such TiO_2 under visible light radiation (Ratova et al., 2018).

From looking into the literature available one can deduce that bismuth oxide would be a suitable match for titanium oxide in the form of a dopant to allow for photocatlytic activation in the presence of visible light, furthermore, bismuth oxide is a suitable sole material for photocatalytic use.

3.0 Methodology- experimental procedure

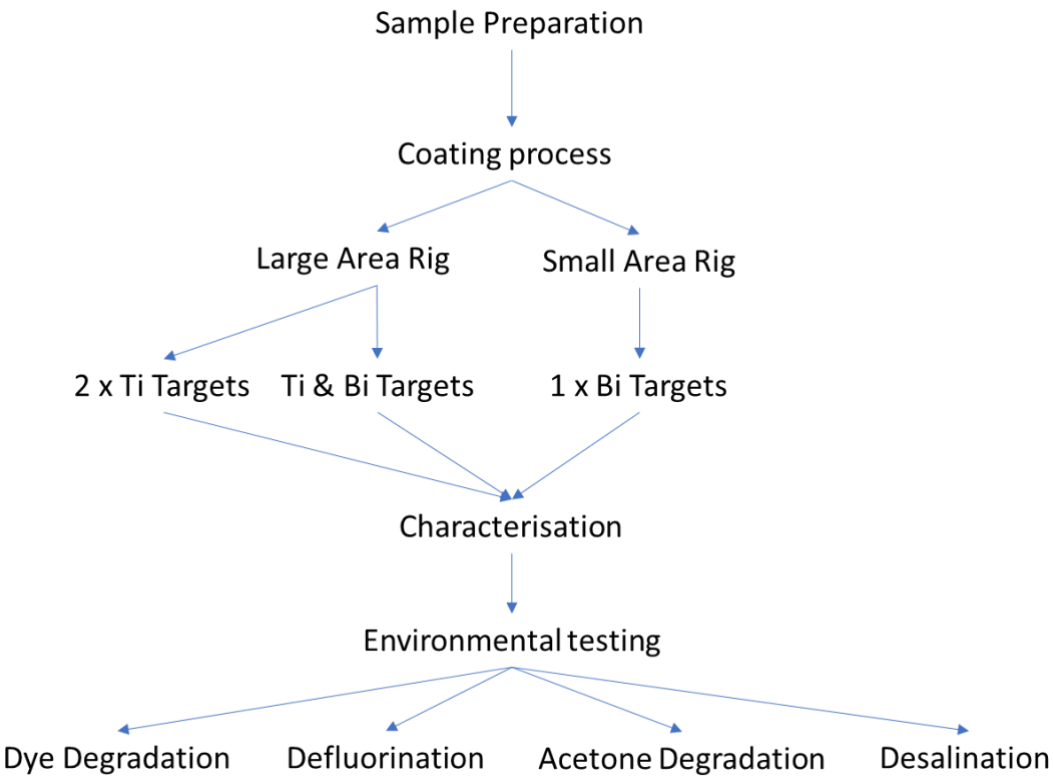

3.1 Substrate Preparation

The substrate in focus is fly ash; however, glass beads were also used to compare photocatalytic activity and the behaviour of the deposited material with the substrate. The substrates undergo preparation before coating to help support better coating and in return better efficiency. There are three different approaches to preparing the substrates: washing with distilled water only or concentrated nitric acid only or a mixture of nitric acid and water.

Concentrated nitric acid was used to remove easily dissolved elements such as CaO. The acid simultaneously etches the surface of the fly ash, with the aim to promote better adhesion between the fly ash and the subsequent coating.

3.1.1 Water only

In a 250ml beaker, 15g of fly ash placed with H_2O added until the fly ash is fully submerged. Using a glass rod the fly ash mixed thoroughly with the water for a few minutes. The mixture is allowed to settle, and filtered using a Buckner flask and funnel. The filtrate, fly ash transferred into a clean beaker and dried overnight in a Carbolite Apex AX30 oven at temperatures of 110°C. This ensures the fly ash is completely dry. The fly ash is ground, using a pestle and mortar to break down any coagulated lumps returning to its original state, fine powder. The final product is transferred to a 28ml sample vial ready to be used for coating.

3.1.2 Concentrated Nitric Acid

Preparing the fly ash with concentrated HNO_3 followed similar steps to 2.1.1. 15g of fly ash added to a 250ml beaker and HNO_3 is added to the fly ash until it is fully covered. The acid and fly ash thoroughly mixed using a glass rod and allowed to settle. Using a clean Buckner flask and funnel to filter off. The fly ash collected is then transferred a clean beaker. The beaker placed on a hot water bath in a fume cupboard overnight helps the fly ash dry, with the evaporated HNO_3 being extracted safely. Once the fly ash is completely dry, the fly ash is ground finely using a pestle and mortar and stored ready to be coated.

3.1.3 Dilute Nitric Acid

Preparing the fly ash with a mixture of HNO3 and H2O followed similar steps to 2.1.1 and 2.1.2. 15g of fly ash is added to a 250ml beaker. A mixture of 120ml of H2O and 30ml of HNO_3 is added to the beaker until the fly ash is fully submerged in the mixture. The fly ash is thoroughly mixed using a glass rod and allowed to

settle before being filtered using a Buckner flask and funnel. The filtrate is then dried overnight in the in the oven at 110°C. The dried fly ash is ground using a pestle and mortar and stored ready for coating.

The method of sample preparation used for the majority of the research was using dilute nitirc acid.

3.2 Coating Process

3.2.1 Magnetron Rigs

During this research two magnetron sputtering rigs have been used, the Large Area rig that operates 2 targets and a small rig that operates a single target. The research had a primary focus of using the large area rig, as there have been no reports of coating CFA with two Ti targets, but with the demand increasing on the large area rig within the department, it was agreed to continue with the small area rig (1 target) to allow for the research to completed utilising a different target beside Ti, since CFA has been coated by Ti as previously mentioned in section 2.2.3 by Yu. It was decided to proceed with Bi as the target of choice with the small area rig, to ensure novelty of the works carried out.

3.2.1.1 Large Area Rig

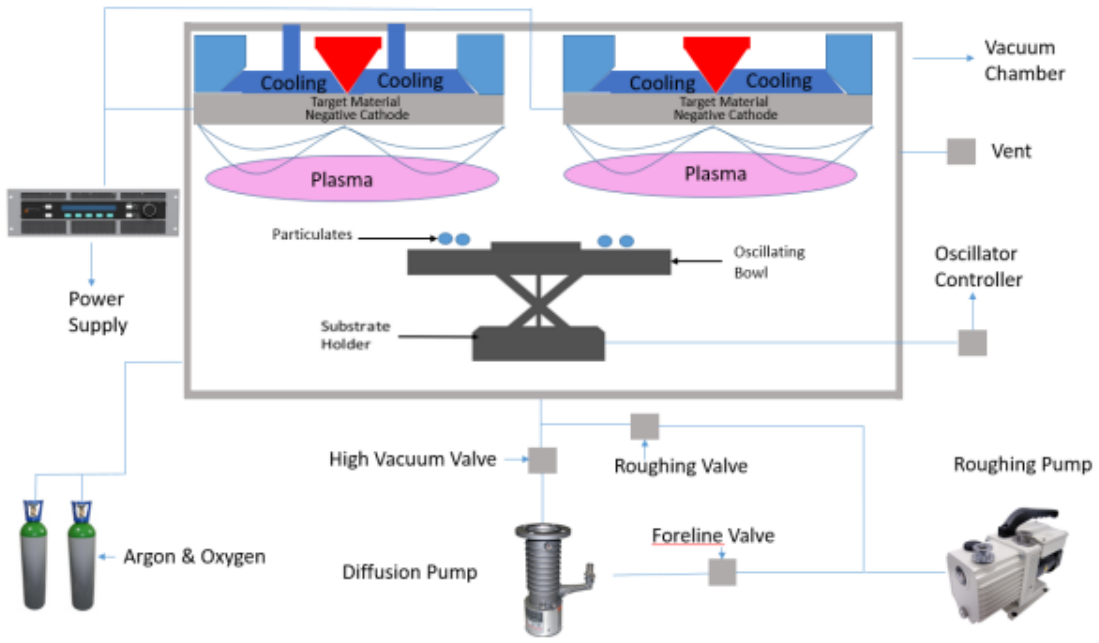

Figure 7: Schematic of the vacuum system of the magnetron sputtering rig used for the coating process.

The large area rig is was built ‘in house’, with dimensions of 1850 x 650 x 300 mm and is predominantly used for TiO_2 coating and coatings with 2 different targets. Several steps need to be followed to ensure vacuum is achieved before a coating can commence. After deciding the target metals to be used, the chamber is brought up atmospheric chamber. The targets are fitted on to 300mm x 100mm Teers Coatings unbalanced type II magnetrons installed in the chambers roof allowing for a sputtering down configuration. The magnetrons are connected to water cooling systems securely to ensure no leaks, before closing the chamber and operating the pumps accordingly to achieve high vacuum and monitored using the Penning gauge and the Baratron. Each magnetron is powered independently by a dual channel ‘Advanced Energy Pinnacle Plus’ pulsed DC power supply.

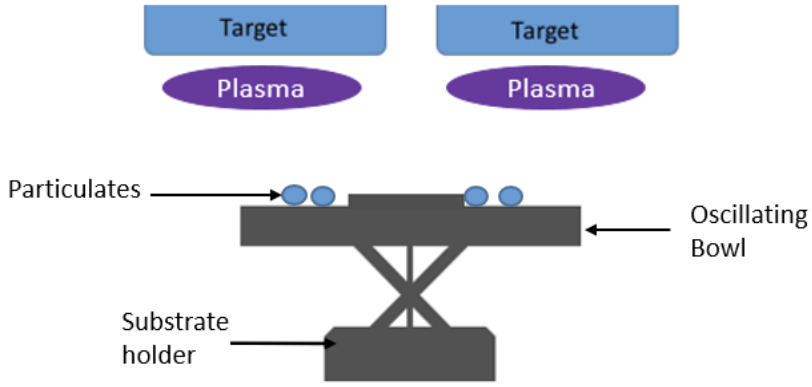

Figure 8: Schematic of oscillating bowl mechanism for deposition of TiO2 using magnetron sputtering.

Figure 9: Images of the oscillating bowl – Original in house substrate holder

The large area rig has space for a substrate holder, the oscillating mechanism to manipulate the substrate (powders-CFA), modified inhouse to allow for the powder CFA to tumble around. The substrate holder was derived from a vibrating bowl feeder, designed for the industrial production lines, it sits approximately 120mm below the two targets the height at which the substrate holder sits can not be adjusted due to the nature of the setup. A stainless-steel substrate holder which initially started as lid with a diameter of 470mm, was used. The modified feeder oscillates at 50Hz vertically, with metal springs bolted from the head of the oscillator to the base at an angle resulting in a lateral twisiting motion of the bowl, thus ensuring the substrate in the bowl is allowed to tumble and roll around the holder and not just bounce vertically, allowing for all the particle surfaces to encounter coating flux over time from both magnetrons. Since the particles in our system tumble about the bowl in and not limited to vertical oscillation, it sets it apart from other powder coating systems that have been reported.

3.2.1.2 Small coating Rig

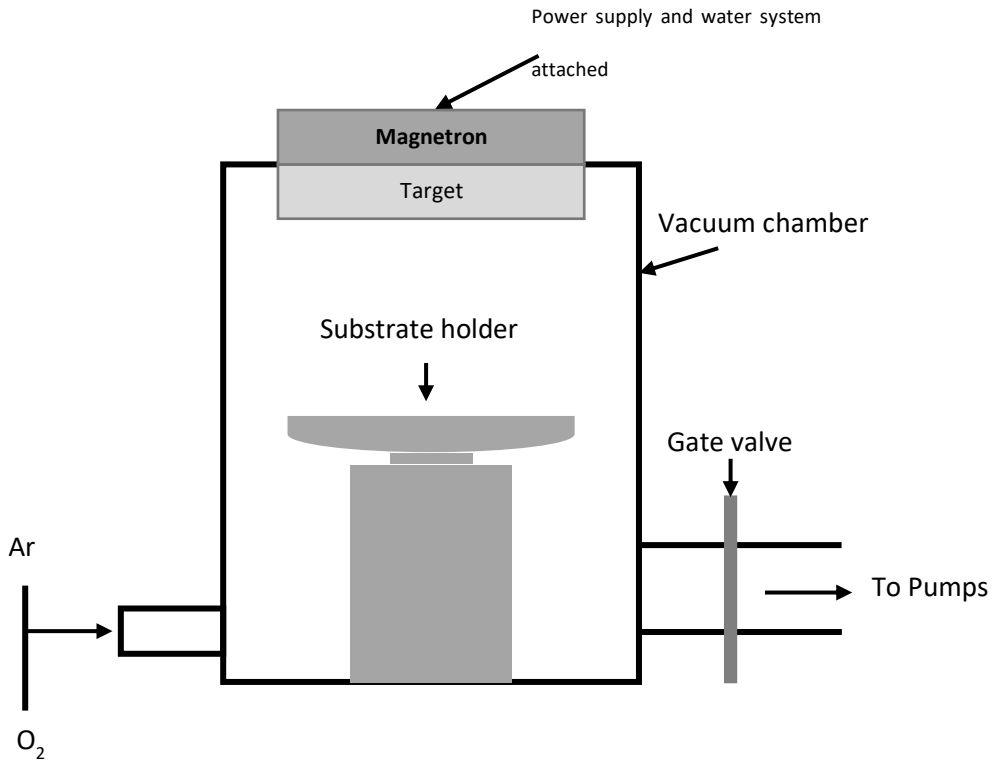

Figure 10: Schematic diagram of the small coating rig, with a single target

Figure 10 is an illustration of the small rig utilised for single target coatings. It was mainly used for bismuth oxide coatings. The small rig adopts the same system as the large area rig, presenting a sputter down configuration, using a single type II unbalanced planar magnetron 7.5 cm in diameter installed on the roof of the sputtering chamber, the chamber has dimensions of 220 x 150 x 150 mm. Hence, the target was facing the substrate holder, composed of a shaker mechanism that allows for the CFA to continuously tumble around; the substrate holder is placed 5 cm underneath the magnetron, the distance between the target and the subastrate holder in this set up much smaller due the size of the rig and as with the large area rig the distance is not adjustable, hence notes have been taken with regards to the distance from the targets has been recorded and the samples are not directly compared. The magnetron was powered by an Advanced Energy

Pinnacle Plus power supply. The chamber is evacuated to pressures below $5x10^{-3}$Pa by means of a rotary pump (Leybold Trivac 16B) and a turbomolecular pump (LeyboldTurboVac i90). The desired pressure was achieved by adjusting the gate valve between the chamber and the turbomolecular pump. Utilising the single target rig became preferable as the availability of the large area rig was limited. The choice to work with bismuth only as a target was made as there have been no reports of bismuth oxide coatings on CFA using a single target magnetron sputtering unlike TiO_2 which has been reported by Yu as detailed in chapter 2.2.3.

3.2.2 Annealing

Annealing is the process that involves heating the material and then gradually allowing it to cool. This process can change the crystal structure of the material, which in turn can influence the material's properties, including its photocatalytic, optical, and electrical properties. Annealing is a process that can further improve the qualities of a material by reducing the number of flaws or impurities present in the material. The annealing process is used predominantly on TiO_2 coated CFA to achieve anatase, a specific crystal structure of TiO_2 that is known to possess photocatalytic properties

The furnaces used were a Carbolite Gero 30-3000°C and Omegalux LMF-3550.

3.2.3 Coating Prameters

This section covers all the coating parameters used to achieve the thin films on CFA. As mentioned in previous sections of the thesis the two targets used are titanium and bismuth. The targets used are of 99.9% purity

The table below includes detailed parameters used for each deposition run and which rig was utilised.

Table 1: details of coating parameters used in the reasearch

Sample Ref	Substrate	Large/Small area Rig	Target A	Target B	Power A - Watt	Power B - Watt	Frequancy - Hz	Pulse - µs	Oxygen flow - sccm	Argon flow - sccm	Coating Duration - hrs	Annealling Temp - ^{o}C	Annealling Duration - min
Sample 1	CFA	Large	Ti	Ti	500	500	100	5	15	15	3	350	30
Sample 2	CFA	Large	Ti	Ti	500	500	100	5	15	15	3	500	30
Sample 3	CFA	Large	Ti	Ti	500	500	100	5	6	15	3	Ramp	30
Sample 4	CFA	Large	Ti	Ti	500	500	100	5	6	15	3	500	30
Sample 5	CFA	Large	Ti	Ti	750	750	100	5	6	15	4	500	30
Sample 6	CFA	Large	Ti	Ti	1000	1000	100	5	6	15	2	0	0
Sample 7	CFA	Large	Bi	Ti	500	500	100	5	6	15	3	500	30
Sample 8	CFA	Small	Bi	NA	500	NA	100	5	6	15	2	500	30
Sample 9	Glass Beads	Large	Ti	Ti	500	500	100	5	6	15	3	500	30

Table 1 details the parameters and conditions of samples discussed in the thesis for ease of referencing. It is not a complete representation of the samples prepared and tested during the duration of this research.

3.3 Analytical Techniques

Several analytical techniques have been employed to characterise the substrate used and the properties of the deposited coatings, to help determine the crystal phase of the samples along with the elements present. Allowing for an educated conclusion or deduction to confirm if the aim of the thesis has been achieved by successfully coating the substrate in question, coal fly ash. The techniques used for analysis and characterisation are:

- X-ray diffraction.
- Raman spectroscopy.
- Scanning electron microscopy.
- X-ray fluorescence.
- X-ray photoelectron spectroscopy with Brunauer-Emmett-Teller Surface Area Analysis.

These analysis techniques predominately rely on surface analysis, which limit in depth analysis of the bulk material.

3.3.1 X-ray diffraction

X-ray diffraction (XRD) is an analytical method to determine the crystalline phase, orientation, and structure of a compound. Crystalline compounds have highly ordered microscopic structures and consist typically of a lattice formed from well-arranged molecules/atoms.

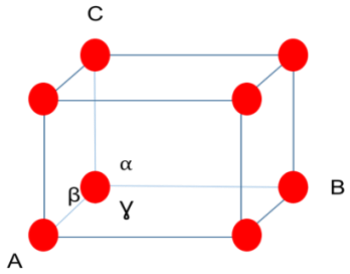

Figure 11: Smallest atomic unit

A unit cell is the smallest box 3-D space description of the atomic arrangement in a crystal structure. The lengths of the unit cells are represented by a, b and c, and the angles between the edges are represented by alpha α, beta β and gamma γ.

The position of the atoms within a unit cell are denoted by the positions on an imaginary x_i, y_i and z_i axis system in which they are measured from a given lattice point. The vectors and the planes in a crystal lattice are described by their Miller index notion (indices); the indices *h,k,l* are directional parameters which are separated by 90°. The syntax (*hkl*) denotes the interception of the plane at a point (axis). If the index is 0, then the plane does not intersect the axis. Plane Miller indices are integers with no common factors. For example, if the atoms are arranged to intersect three axis *hkl* would be (111), if the arrangement intersected 2 axis *hkl* could vary between (011, 110 or 101) and if the arrangements only intersects 1 axis *hkl* would be (100, 010 or 001) (Brundle et al., 1992).

The peaks generated in XRD are a result of the constructive in-phase interference; In order for a peak to be generated (maxima) the wavelength of the X-ray needs to be in phase, and this occurs when the extra distance travelled by the diffracted beam is a multiple factor (integer) of the 1st beam wavelength; The X-rays are emitted at angle of θ towards the sample. Upon interacting with the electron in the atom the X-ray is diffracted at the same angle θ. As the sample would have different planes, a simultaneous X-ray would interact with the electron on the atoms on the second plane of the sample with the same angle of θ, and also be diffracted with the same angle θ. The second X-ray wave would need to travel further to reach the second plane of the sample, hence, the difference between the two waves is the extra distance travelled. The extra path length travelled by the 2nd wave is equal to dSinθ, where *d* represents the spacing between the two planes. The angle on the incident beam to the plane is θ. As mentioned earlier in order for a peak to be detected the wavelengths need to be in phase, hence they would fit Bragg's equation, where *n* is the multiple factor (integer) and *d* is the interatomic distance.

[Eq.3] Bragg's equation: $n\lambda = dSin\,\theta$

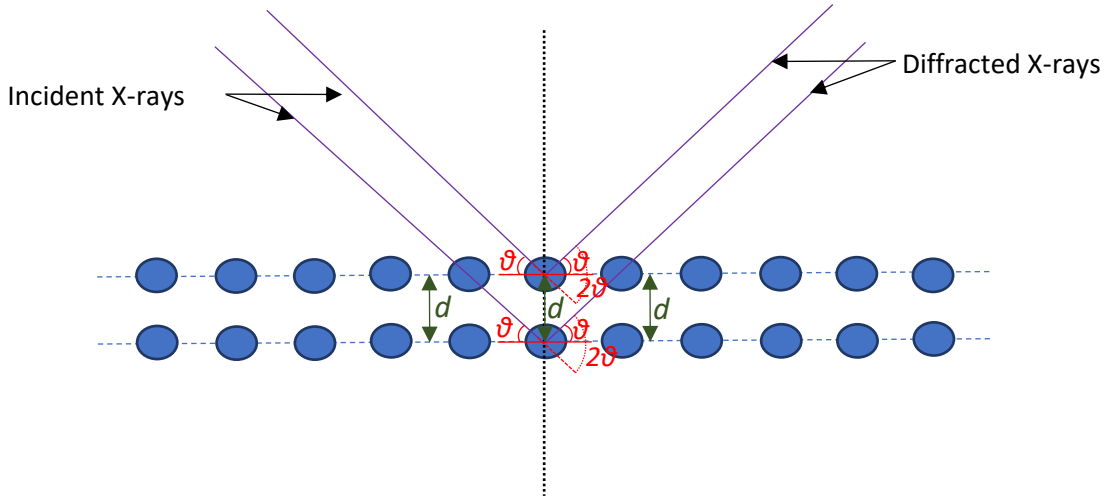

Figure 12: A schematic representation of X-ray diffraction, d=Interatomic distance

The XRD instrument is set up so the detector is able to record the X-rays that have been diffracted. The detector is attached to a device that measures the angle at which the detector is at, enabling the calculation of the interatomic spacing *d*. The peaks generated are plotted as a function of angle 2θ, hence each position will detect a specific X-ray. The intensity is recorded as counts and increases as the wavelength is amplified. The final trace/plot of X-ray peaks are then compared to a reference database to determine the properties of the sample in question (Brundle et al., 1992). The XRD method of analysis excels when the subject being analysed is crystalline in structure and has a high sensitivity to structural changes which reflects the quantity and composition. However, XRD is faced with a numberof limitations including indepth analysis, the analysis is limited to surface analysis. XRD will not be able to analysis amorphous samples, nor will it be able to distinguish overlapping peaks unless there are shifts in structures.

A PANalytical Xpert3 MRD X-ray diffraction system (PANalytical LTD, Cambridge) was used in this research. The start angles chosen were 20° or 10° and the final angle is 89°, with step size set at 0.039° and the time is 0.9s per step. The voltage and current used to generate the X-rays from a copper filament are 40kV and 30mA respectively. The collected data would then be interpreted using 'Highscore' software supplied by PANalytical LTD. The data is then exported in a “csv” format to Microsoft excel allowing for the data to be studied closely and replotted. This specific XRD instrument allows for a hot-stage to be used during the analysis of the sample. The sample that is placed in the holder is annealed to the required temperature and analysed. Pre-setting the temperature increments and the final temperature allows for the study of temperature effects on the structure of the sample.

3.3.2 X-ray fluorescence

X-ray fluorescence, often known as XRF, is a method of analysis utilised to ascertain the elemental makeup of a given material. It requires X-rays with a high intensity to excite the atoms in a sample; causing the atoms to release secondary X-rays specific to the elements present in the sample. The sample elemental composition can be determined by detecting and analysing the secondary X-rays emitted from the sample.

The X-ray fluorescence (XRF) approach is a non-destructive method, which allows to analyse samples without the need to be destroyed or changed in any way, it can limit the analysis as it is restricted to surface analysis only of a non destructive nature. It finds wide usage in a wide range of applications, including the examination of soil, water, and air samples, in addition to the study of industrial materials, such as metals and alloys, among other things. The XRF process may be utilised to analyse cultural artefacts such as paintings, old coins, and geological materials.

X-ray fluorescence (XRF) is a method for identifying the elemental composition of a sample that is both quick and accurate, and its cost is comparatively modest compared to the costs of other analytical techniques. However, it is not sensitive to all elements, and detecting some elements may require additional steps, such as processing samples or using specialised detectors (Brouwer, n.d.).

The high energy incident X-ray is used to ionise the atoms in the sample. Ionisation can only occur when the radiation's energy is higher than its ionisation energy. This causes one electron to be removed from the atom's inner orbital, which is the outcome of ionisation. During this process, an electron from a higher

orbital is used to fill the vacant space, and as a result, a photon is produced. The difference in energy between the two orbitals is what we refer to as the photon's energy. The emission of the fluorescent photon is caused by the movement of the electron from the L orbital to the K orbital (characteristic X-ray). The photon emitted is one of a kind and is particular to the atom that is now present; in addition, the strength of the radiation discharged represents the quantity of a specific element existing in the substance (Flewitt and Wild, 2017).

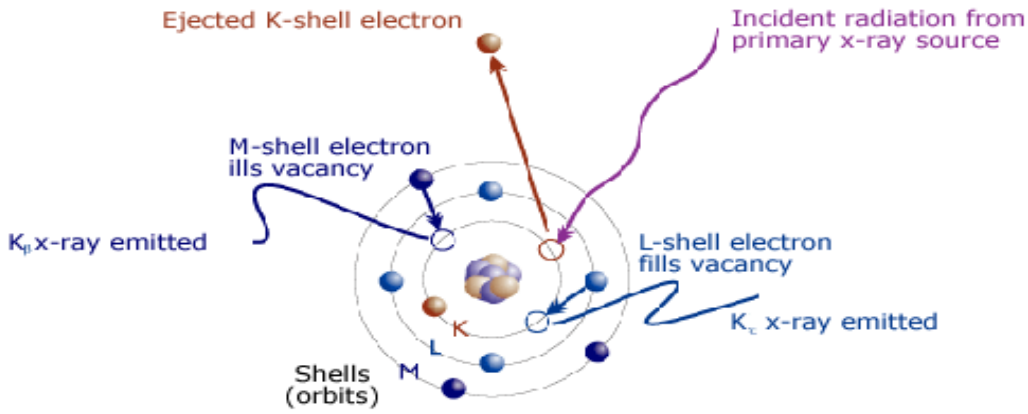

Figure 13: XRF excitation diagram (*XRF Schematic*, n.d.)

3.3.3 Raman spectroscopy

Raman spectroscopy is an analytical technique used to determine the structural properties of a given material; the process was introduced in the 20th century by Sir C V Raman. This method facilitates unknown materials to be detected by comparison of the spectral fingerprint produced against a reference database. The technique is used for several reasons, including the ability of in-situ analysis, its non-destructive nature, and quick analysis duration.

The process relies on detecting scattered photons, namely stokes and anti-stokes scattering. Scattering is the process in which the light source is absorbed and re-emitted in a different direction, generally observed at right angles. This is due to a difference between incoming radiation energy and the separation energy of the molecules.

The base of the analysis is the energy difference of the photon. As mentioned earlier, Rayleigh scattering occurs when the photon is scattered with its original energy following excitation and relaxation, as illustrated in the diagram below. The second instance is when the photons are excited to the virtual state and relaxed to a higher vibrational level than the original. The molecule has gained energy, resulting in an inelastic scattering known as Stokes scattering, less energetic than the incident photon (lower frequency). The final kind of scattering is when photons are excited to a virtual state and relaxes to a lower vibrational state than the original vibrational state indicating the molecule has lost energy resulting the photon scattered having more energy than the incident photon. This is referred to Anti-Stokes scattering that has a higher frequency (Flewitt and Wild,

2017)(Brundle et al., 1992). The data obtained in a spectral graph illustrates the Raman shift in wavenumbers and expressed in cm^{-1} against intensity “count rate”. Raman spectroscopy works well in analysing the coated fly ash to determine the crystal structure of photocatalytic coatings. The limitation faced with Raman spectroscopy is is the sensitivity to low concentration and depth analysis. making it predominantly surface analysis.

The instrument used for Raman spectroscopy was a ThermoFisher scientific DXR Raman microscope with a 532 nm laser at 1 mW, 50x LWD microscope, 900 lines per mm grating, an estimated spot size of 1.1 µm and a 25 µm pinhole. All spectra data obtained were compared to a database of standard spectra provided by ThermoFisher scientific to analyse the crystallography of the materials present.

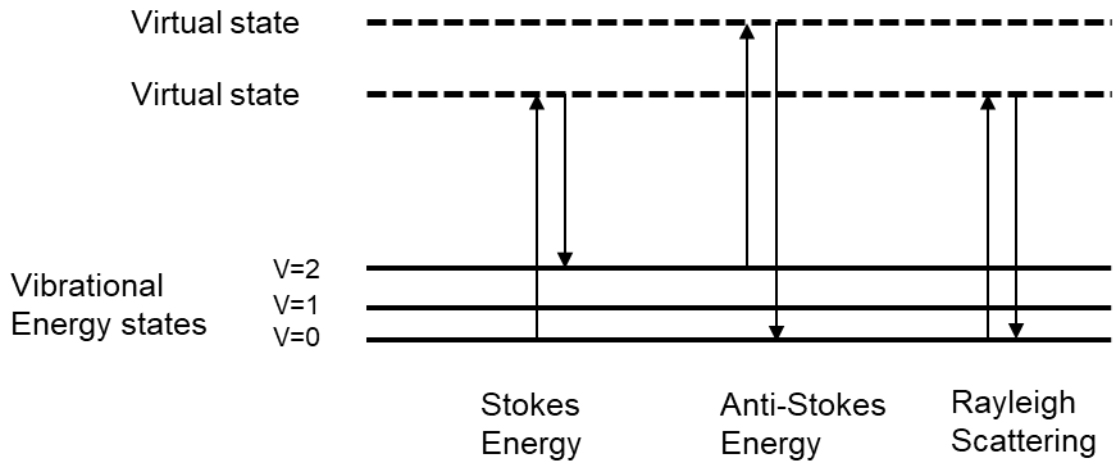

Figure 14: Transitional energy levels of absorption and desorption of energy in Raman spectroscopy

3.3.4 Scanning electron microscope

Scanning electron microscopy, commonly referred to as SEM, is one of the most common analytical tools across many science and engineering disciplines. The technique capable of generating high-resolution images at magnifications of up to 500,000x, this physiochemical technique relies on firing a concentrated high-energy electron beam at a sample with energies ranging from 5 to 30 kV. It is used to visualise the surface at a high magnification and depth of focus which optical microscopes cannot achieve, giving a topographical image of a material. Energy dispersive x-ray spectroscopy (EDX or EDS) can also identify the elemental composition at a sample's surface. This technology varies from an optical microscope because it detects light, whereas scanning electron microscopy creates and detects electrons. Optical microscopes rely on lens technology to attain high resolutions (the limit of resolutions is defined as the shortest distance at which two objects can be observed apart). However, this can only reach around 200nm. SEMs can attain a resolution of 0.9nm utilising electrons, whereas the human eye can only achieve a resolution of 0.1mm at most. EDX can also be used to examine the elemental makeup. Electrons are shot at a material's surface and interact in various ways. As a result, photons, electrons (backscattered electrons and secondary electrons), and x-rays are produced, hitting various detectors, and finally generating an image. An electron gun, electron lenses, apertures, a stigmator, electron detectors, a vacuum system, scanning coils, a specimen holder, and a specimen stage are all part of a scanning electron microscope's configuration. A vacuum environment is required for the SEM to function correctly. The accelerating voltage, spot size,

aperture, and working distance are all SEM operating parameters (Brundle et al., 1992; Ratova, 2013; Flewitt and Wild, 2017)

3.3.5 X-ray photoelectron spectroscopy

X-ray photoelectron spectroscopy (XPS) is a surface-sensitive quantitative spectroscopic technique that measures the elemental composition at the parts per thousand range (Shard, 2014), electronic state, empirical formula and chemical state and of the elements that exist within a material.

XPS alternatively referred to as electron spectroscopy surface characterisation, is a technique for examining thin surface layers. XPS bombards the sample with well-defined energy X-rays, typically from an Al K or Mg K source with kinetic energies of the electrons typically in the range of 300 to 1500eV (Son et al., 2020). The X-rays interact with the core electrons surrounding the nuclei of the various atoms present on the sample's surface, resulting in the emission of a photoelectron. The kinetic energy (KE) of these emitted electrons is characteristic of the photoelectron's parent element. Each electron in an atom has a unique binding energy, which is quantified and analysed. The location and intensity of the peaks in the resulting energy spectrum provide quantitative information about the desired chemical state. To quantify the binding energy, photoemitted electrons' kinetic energy is measured using a detector, and electrons emitted from the material's top 1^{-10} nm are analysed (Fadleys, 2009).

$$[\text{Eq 4}]: BE = hv - KE$$

The above equation illustrates the relationship between the photoelectron's measured kinetic energy (KE), the binding energy (BE) and energy of X-ray photon hv. By counting ejected electrons over a range of electron kinetic energies, a photoelectron spectrum is obtained. The photoelectrons peak

energies and intensities enable the identification and quantification of all surface elements except hydrogen, which lacks inner shell electrons. Rather than that, hydrogen has a 1s electron that is a valence electron, and thus any signal from hydrogen will overlap with signals from the excitation of valence electrons from other surface atoms, as the binding energies of valence electrons vary significantly. XPS can determine an element's composition, empirical formula, chemical state, and electronic state (Ratova, 2013; Isaacs et al., 2021).

XPS analysis was performed by MMU analytical services team namely Gary Miller with an AMICUS photoelectron spectrometer (Kratos analytical AXIS Supra+) equipped with Mg K X-rays as the primary excitation source. The binding energy was referenced to the C 1s line at 284.8 eV for calibration. Curve fitting was performed applying a Gaussian function with a Shirley background. The detector was a hemispherical analyser coupled to a delay line detector, operating with a 110 μm aperture in the lens column with the lens operating in the FOV2 mode with a resolution of 40 eV.

3.3.6 Brunauer-Emmett-Teller (BET)

Brunauer-Emmett-Teller (BET) method is used to determine the surface area of a sample based on gas adsorption, as shown in. At -196°C (nitrogen's boiling point), nitrogen gas is below the critical temperature and thus condenses on the sample's surface. Assuming that the gas condenses onto the surface in a monolayer, the amount of adsorbed (condensed) gas is correlated to the total surface area of the sample, including pores. The application of the BET equation, which was derived more than 65 years ago, is one of the most common methods

for calculating the specific surface area. Surface area determination based on the BET theory is an application of the BET equation, see [Eq 5], where X is the weight of the as adsorbed, P/Po is the relative pressure, Xm is the monolayer capacity, and C is a constant 145.

[Eq.5]: $P/PoX[1-(PP0)]=1XmC+C-1XmC(PP0)$

The general procedure for performing a BET surface area measurement is as follows: first, a sample within a tube is degassed by heating and evacuating or by adding nitrogen. The sample and the reference tube are then evacuated. At this point, the majority of methods will perform a dead volume measurement using an inert gas such as He to ensure that the dead volumes of both tubes are comparable. The dead-volume gas is subsequently pumped out. Next, the adsorbate gas is introduced into the two tubes, whereupon the sample absorbs the gas and the pressure in the confined volume decreases until the adsorbate gas and adsorptive gas reach equilibrium. Therefore, the quantity of adsorbate gas at equilibrium pressure is the difference between the quantity admitted and the quantity remaining in the gas phase. The collection of several data points is required. The P/Po ratio must fall within the range of 0.025 to 0.30 in order for the BET equation to accurately calculate the surface area. At relative pressures greater than 0.5, capillary condensation begins, while at low relative pressures, only monolayer formation occurs. When the BET equation is plotted, the gradient of the graph should be positive. If no such graph is obtained, the BET method was unable to determine the surface area. Using least-squares regression, one can obtain the slope and y-intercept (Ambroz et al., 2018).

3.4 Testing methods.

Several methods have been adopted to determine the effectiveness of the coated CFA in environmental process. Depending on the method used a conclusion may be drawn with regards to the possibility for further research and potentially scale to a commercial level for organic compound degradation in water treatment, fluorine levels regulation, desalination for potable water.

3.4.1 Dye degradation

A primary aim of the research is to is determine if the coated fly ash can be used in organic pollutant degradation. There are different organic, catanionic and anionic dyes that contribute to, or model environmental water pollution. Some of them are widely described in the literature, such as methylene blue MB, methyl orange MO, rhodamine B,malachite green . The primary focus was the organic cationic dye methylene blue, as an indicator for photocatalytic catalysis along with organic anionic methyl orange dye. The same set up was applied to both dyes (Sayilkan et al., 2008; Andronic et al., 2009; Saepurahman et al., 2010).

Photocatalytic activity can be determined by a relatively straightforward method. The bases of the experiments are the degradation of the dyes under a light source, be it ultraviolet UV, solar light or fluorescent light. The dyes used have different colours allowing for their degradation/oxidation can be observed by measuring the absorption of the solution at specific wavelengths. One of the most common dyes used to evaluate the capabilities of photocatalytic surfaces is MB. MB is used to evaluate new photocatalytic materials, photoreactors, and light source performances. The use of MB as an organic dye for assessing the photocatalytic activity of surfaces in an aqueous solution is confirmed by ISO

standard 10678 (Ratova, 2013; Ambroz et al., 2018). MB is a common water pollutant due to the heavy demand in the textile and printing industry. Experimenting with the CFA for the degradation of the MB will indicate the potential use in wastewater treatment. MB is aromatic in structure and holds a molecular formula of $C_{16}H_{18}ClN_3S$; in an aqueous solution, it has an absorption peak of 665nm. The right dye concentration must be used to allow the photons from the light source to pass through to react with the surface of the photocatalyst (Mitoraj et al., 2018).

MO is an anionic dye used as a pH indicator with a molecular formula $C_{14}H_{14}N_3NaO_3S$. MO can be broken down by means of oxidation as a result becoming colourless, and the absorption peak of MO is 464nm. The steps of experiment are the same as described below for MB.

In a 200ml beaker 100ml of diluted MB was added. The 1ml aliquot (before the addition of the coated sample) was tested for absorption using a UV-Vis spectrophotometer and returned to the original beaker. The coated sample would be immersed in the MB solution for 30 min to saturate the surface along with a stirrer bar to reach equilibrium, during this time the beaker would be covered to prevent any activation as a result of visible light. Once the 30-minute period is over the lid is removed and the UV lights are switched on above the beaker. The beaker rests on a magnetic stirrer, which agitates the coated substrate with MB. 1ml aliquot would be taken and tested this procedure would be repeated 5 times once every hour unless stated otherwise. The anticipated results would be a decrease in absorption; the higher the concentration of the MB solution the higher the absorbance would be. Hence, as the MB degrades the absorbance would

also decrease, as result of the formation of colourless productions from the oxidation of MB via the strong oxidizing radicals.

$$C_{16}H_{18}ClN_3S + 25.5O_2 \xrightarrow{TiO2 + h\lambda} HCl + H_2SO_4 + 3HNO + 16CO_2 + 6H_2O$$

[Eq 6]: Methylene Blue degradation

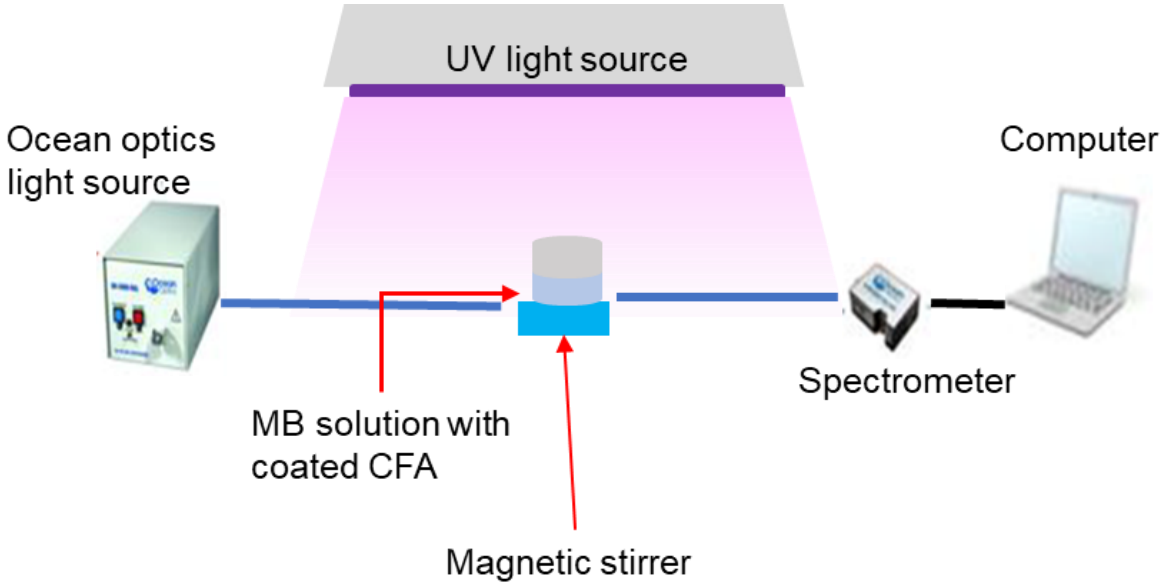

Figure 15:Schematic diagram of the Dye degradation setup

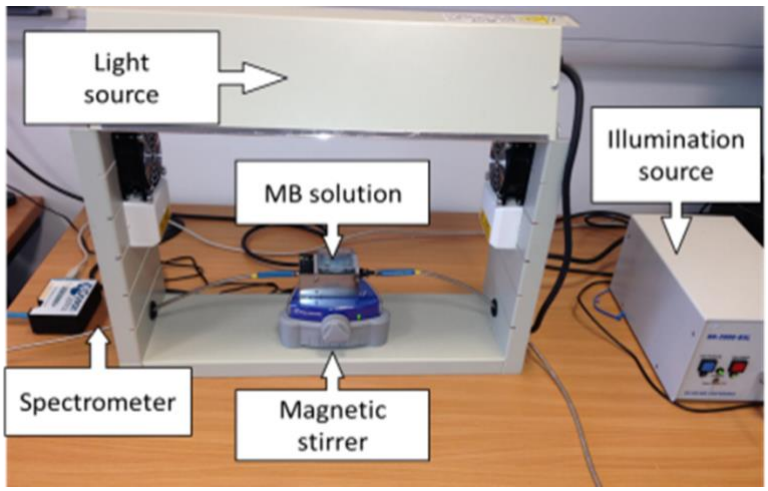

Figure16: Image of dye degradation setup in the laboratory

The absorption peak height was monitored using Ocean Optics USB 2000+ miniature spectrometer connected to deuterium-tungsten illumination source DH-2000-BAL via fibreoptic cables.

3.4.2 Defluorination

Defluorination is a process by which fluoride ions are removed from the water or any other fluid. Fluoride is a chemical compound soluble in water naturally present from natural water sources. Nonetheless, fluoride may be added to public water supplies to help prevent tooth decay; in the UK, fluoride levels are around 1mg per litre. On the other hand, high levels of fluoride may result in several health problems (Ambroz et al., 2018).

Different methods may be adopted to help regulate the levels of fluorine by removing or adding fluorine; this section focuses explicitly on the reduction of fluorine. The standard techniques vary from physical, chemical, and biological. Physical methods involve filters, membranes, or other mechanical processes to remove fluoride from water. Chemical methods include using chemicals to bind or precipitate fluoride ions, while biological methods involve using microorganisms or plants to remove fluoride from water.

Adsorption is the most common physical technique, which entails the removal of fluoride ions from water molecules by binding onto materials such as bone char and activated alumina, known as "adsorbent materials". Precipitation is another method adopted in the industry for fluoride ion removal from water by forming a solid residue and is filtered off, along with ion exchange where the fluoride ions are exchanged for other elemental ions. Fluoride ions present in water occur if the right conditions are present when the fluoride ions dissolve into the ground water from the rocks present in the vicinity. Fluoride compounds vary including

fluorapatite $Ca_5(PO_4)_3F$, fluorspar CaF_2, cryolite Na_3AlF_6 and Sellaite MgF_2 (Bhatnagar et al., 2011).

Fluoride can also come from industrial effluents with high fluoride levels (Mohapatra et al., 2009). Several industries are responsible for high fluoride levels in wastewater include: beryllium extraction, Electroplating, ceramic production aluminium smelting, and coal-fired power plants.

According to WHO the suggested levels for human consumption of fluoride is $1.5mgL^1$. Half of the fluoride humans are exposed to is stored in teeth and bones, while the rest returns to the environment. Fluoride concentration within the guidelines of WHO help with maintaining good human health by preventing tooth decay, strengthening the enamel. Levels greater than the guideline cause bone hardening and embrittlement along with dental fluorosis (Meenakshi and Maheshwari, 2006).

Wastewater with high levels of fluoride levels may be of detriment to the ecological system it contacts. Fluoride levels are known to alter the conditions in the soils of farmland deeming them not suitable for vegetation. Along unwanted poisoning to the waters due to the high levels of fluorine, potentially killing marine life.

Several approaches may be taken to minimise fluoride levels from becoming too high is to use different modes of transport, pretesting the levels of fluoride and counter the levels with low fluoride water or possible even rainwater to dilute the concentration. If these approaches are not viable then a defluorination processes is a must. As mentioned earlier a few methods may be used to achieve defluorination, each process has its pros and cons. Meheshwari reports the use

of activated alumina, activate carbon and titanium for the process of absorption (Meenakshi and Maheshwari, 2006).

This experiment is to determine the fluorine absorption capability of coated CFA in collaboration with the University of Witwatersrand South Africa using our TiO2 CFA. Tests have reported that commercial TiO_2 has an absorption of 30mgFkg^{-1}, while CFA can absorb 0.28mgFkg^{-1}.

3.4.3 Desalination

As mentioned earlier in the thesis, potable water is becoming scarce, with the demand of the clean, fresh potable water is at an all-time high. The only means to tackle the issue is with innovative solutions and know methods, as this issue will only increase with time as the demand continues to increase. Recent years have seen an increase in the level of attention scientists pay to resolving the freshwater conundrum due to the scarcity of potable water, particularly during extended periods of drought. Only 2.5% of all water sources are fresh water, with 80% of this quantity being frozen in the icecaps or blended as soil moisture; on the other hand, around 97.5% of all water sources are salt water predominantly from the oceans. Unfortunately, it may not be used in its original condition without undergoing treatment to become suitable for use. There are several methods currently used such as thermal distillation. However, this technique has drawbacks due to the high-power consumption which main relay on non-renewable power supply, which can reflect a high cost for such process. This leads scientist to work tirelessly to reduce cost of the process. Several scientists including Garcia-Rodriguez have explored the possibility to power the process of desalination using renewable energy. One of the proposed methods is solar

powered desalination, initial investigations indicate positive results of producing fresh water.

This research aims to investigate the possibility of using coated CFA as a photocatalyst in the process of desalination, ultimately a low-cost method for desalination. The photocatalytic desalination of saltwater has yet to be researched in depth (Emadzadeh et al., 2014; Pouyfaucon and García-Rodríguez, 2018).

The procedure predominantly measures the conductivity of the saltwater at the start and monitor the results periodically. Along with conductivity the turbidity and the pH of the water is tested and compared to help understand the nature of the reaction that occurs. The instruments used for determining conductivity, pH and turbidity are: Jenway 4510 conductivity meter and Jenway 3510 pH meter.

3.4.4 Acetone Degradation in a closed chamber

$$C_3H_6O + 4O_2 \xrightarrow[h\nu > 3.2eV]{TiO_2} 3CO_2 + 3H_2O$$

[Eq 7]: Acetone degradation reaction

The decomposition of acetone produces carbon dioxide. In this experiment, 3ml of acetone was introduced to the chamber holding 5g of coated sample. The chamber/ vessel would be appropriately secured; the top of the vessel houses a glass opening to allow for the UV light to pass through and activate the coating. Equilibrium is reached before allowing the UV rays to react with the coated samples by covering the glass window to prevent any visible light or UV light from triggering any unwanted activity.

A Vaisala CO2 probe and counter are used to determine the concentration of CO2 in parts per million (PPM). The gathered data is presented as a graph on the handheld terminal or as a table; unfortunately, the data cannot be exported to another device to be displayed. The diagram should demonstrate a positive increase in concentration and level out as the acetone is fully degraded.

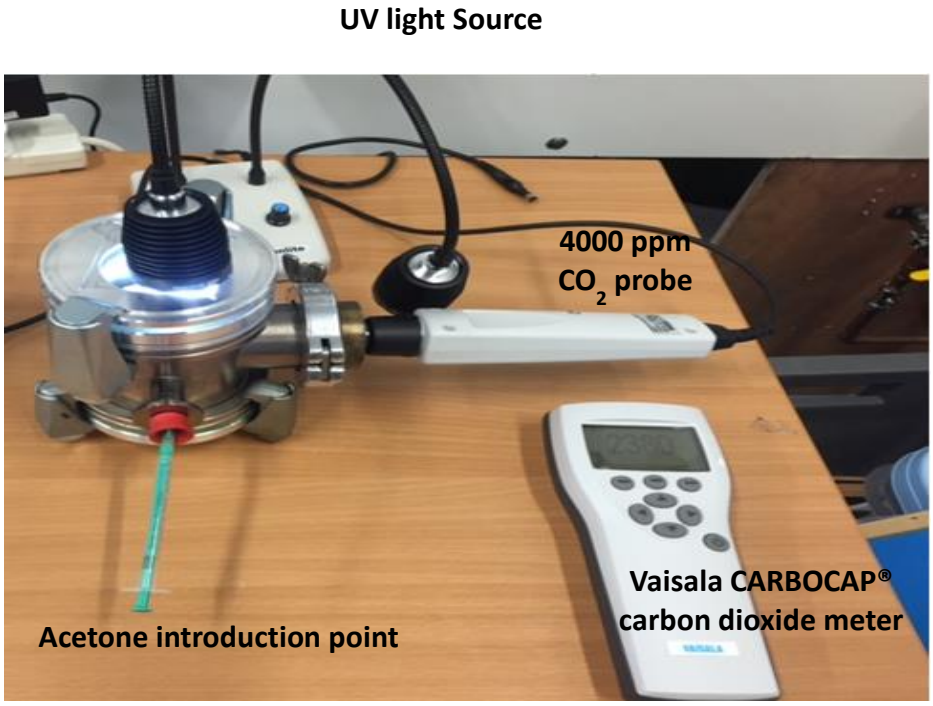

Figure 17: Acetone degradation testing set up

4.0 Results and discussion

This chapter covers the results achieved from the various characterisation and testing methods conducted.

4.1 Titanium Dioxide deposited using large area rig

4.1.1 Sample characterisation

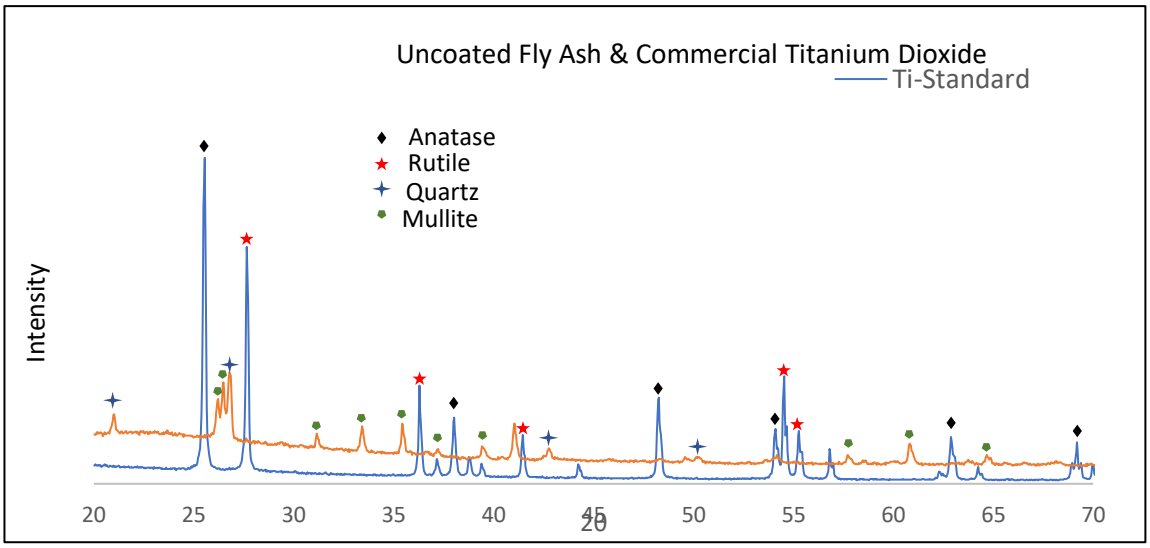

Figure 18: XRD patterns TiO_2 PC500 standard and uncoated CFA

Figure 18 illustrates the XRD pattern comparison between uncoated CFA and commercially available PC500 TiO_2, the XRD pattern corresponds with anatase and rutile. The reason behind comparing the two XRD patterns is to determine if there are any visibly overlapping peaks, as the initial XRD analysis of the TiO_2 coated CFA did not_exhibit any clear definitive peaks of TiO_2. By comparing individually the XRD patterns of the CFA and titanium dioxide allows for better understanding the patterns. The TiO_2 coated CFA has been analysed and characterised. The XRD graphs below represent the as deposited TiO_2. There are no visible TiO_2 peaks, this potentially maybe attributed to a number of factors including the structure of TiO_2 not being crystalline or overlap of the peaks along with the amount of TiO_2 deposited on the surface.

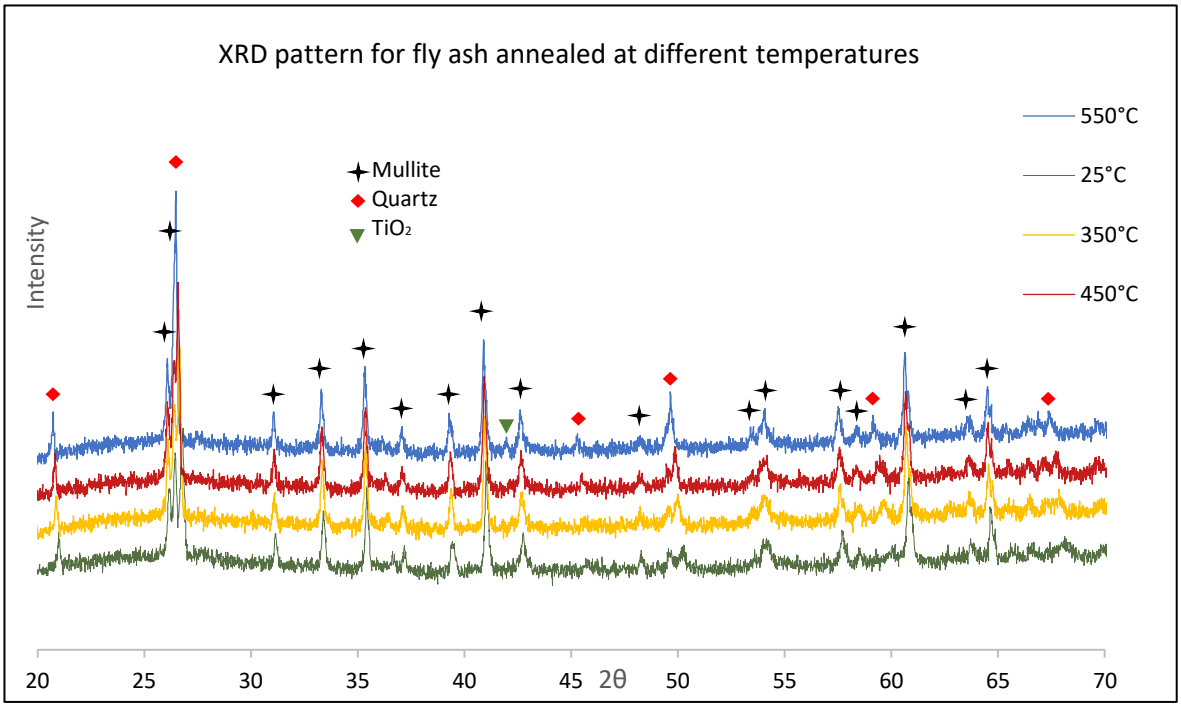

Figure 19: XRD patterns for annealed TiO2 coated CFA annealed at different temperatures.

Figure 19 is a compilation of XRD patterns from sample 3 annealled at different temperatures. The CFA (sample 3) was analysed with the aid of the hot stage, a platiunum insitu heating platform to determine if with the increase of temperature (annealing) could alter the crystal phase resulting in a change in the XRD pattern. From figure 19 one can deduce that increasing the temperature impacts the XRD pattern of the TiO_2 coated CFA even though the change is minimal. Conducting further analysis using SEM EDX one can confirm that TiO_2 was successfully coated onto the CFA.

Table 2: EDX wt% for uncoated CFA

Element	Wt%	At%
CK	01.84	03.11
OK	48.21	61.20
NaK	00.15	00.14
MgK	00.68	00.56
AlK	21.03	15.83
SiK	23.80	17.21
KK	00.42	00.22
CaK	02.06	01.04
TiK	00.55	00.23
FeK	01.26	00.46
Matrix	Correction	ZAF

Table 3: EDX wt% for Sample 4

Element	Wt%	At%
CK	11.72	19.40
OK	37.57	46.69
NaK	00.36	00.31
MgK	00.52	00.43
AlK	17.43	12.84
SiK	23.29	16.49
KK	00.81	00.41
CaK	02.01	01.00
TiK	03.35	01.39
FeK	02.66	00.95
CuK	00.28	00.09
Matrix	Correction	ZAF

Comparing tables 1 & 2 one can see the increase in elemental composition of titanium from 0.55% to 3.35%, respectively for uncoated CFA and sample 4.

The samples were sent for surface area calculations by means of BET with the aid of Dr L.Tosheva, but unfortunately the technique was not suitable as per the feedback from Dr Tosheva “he surface area of these samples is very low and not meaningful, the correlation coefficients for the results are not acceptable”.

XPS analysis for sample 4 further confirms the successful deposition of TiO_2 on to the surface CFA. Figure 20 illustrates the XPS narrow spectra of Ti_{2p} of the surface of the TiO_2 coated CFA. The binding energies of Ti $_{2p3/2}$ and $Ti_{2p1/2}$ were observed to be 459.26 and 464.97 eV respectively. The binding energies were attributed to the $Ti^{4+}(TiO_2)$ according to literature.

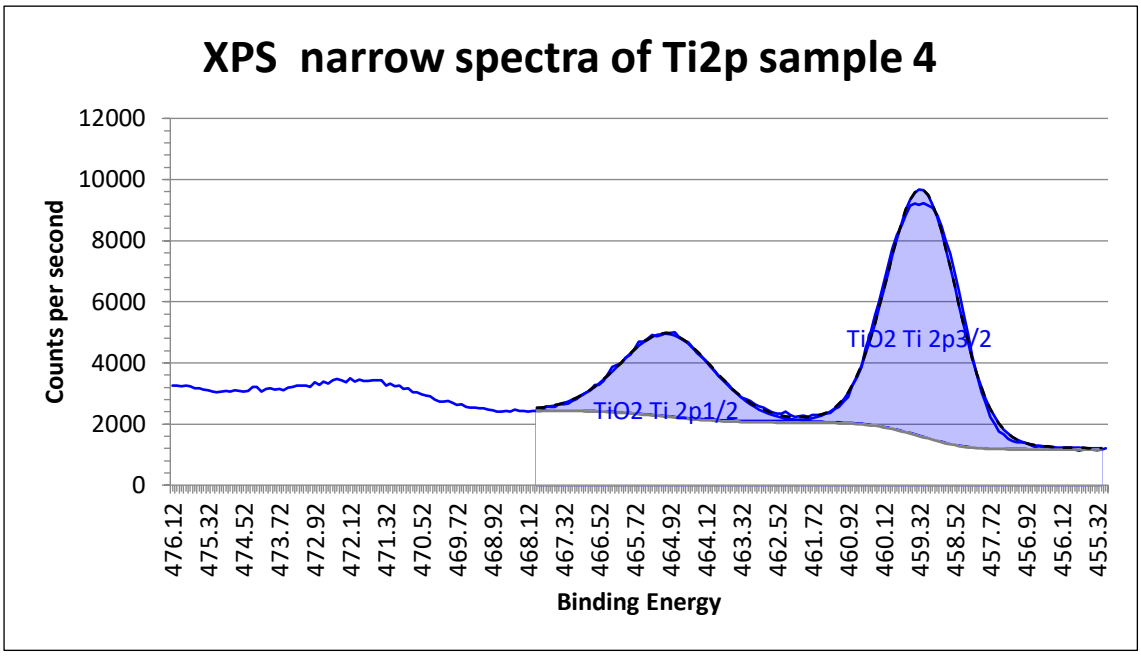

Figure 20: XPS narrow spectra of Ti_{2p} for deposited Titania

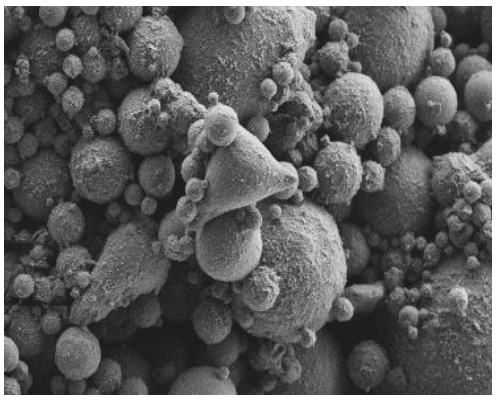

Figure 21: SEM image of sample 4 10.0kX

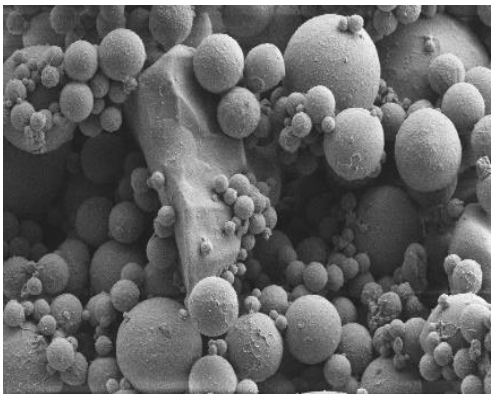

Figure 22: SEM image of sample 5 10.0kX

Figure 21 and 22 are images of obtained from SEM analysis comparing both images of TiO_2 coated CFA sample 4 and sample 5 at the same 10000 magnification. No clear visible differences are apparent within the images.

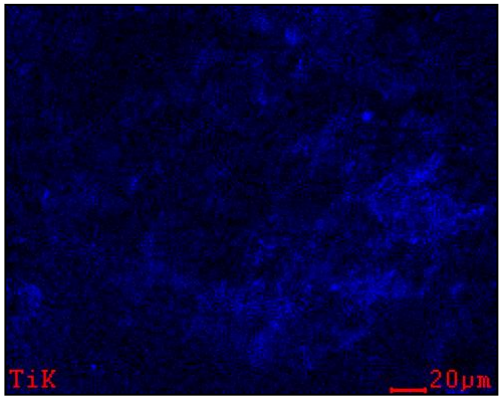

Figure 23: SEM-EDX map image of sample 4

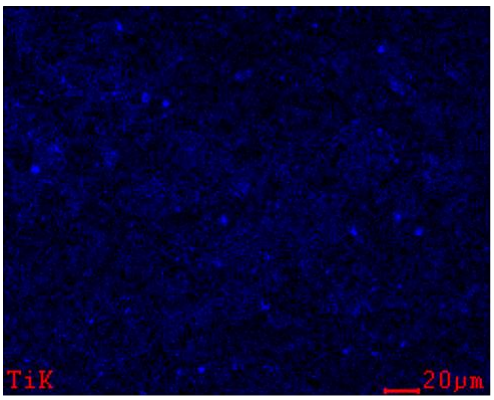

Figure 24: SEM-EDX map image of sample 5

Figures 23 and 24 illustrate mapping of Ti specifically in both samples 4 and 5 respectively. It can be noted that Ti has been deposited across the surface of CFA, however, not in a uniform manner. This can be attributed to the nature of CFA and the method of coating using the substrate holder described in section 3.2.1.

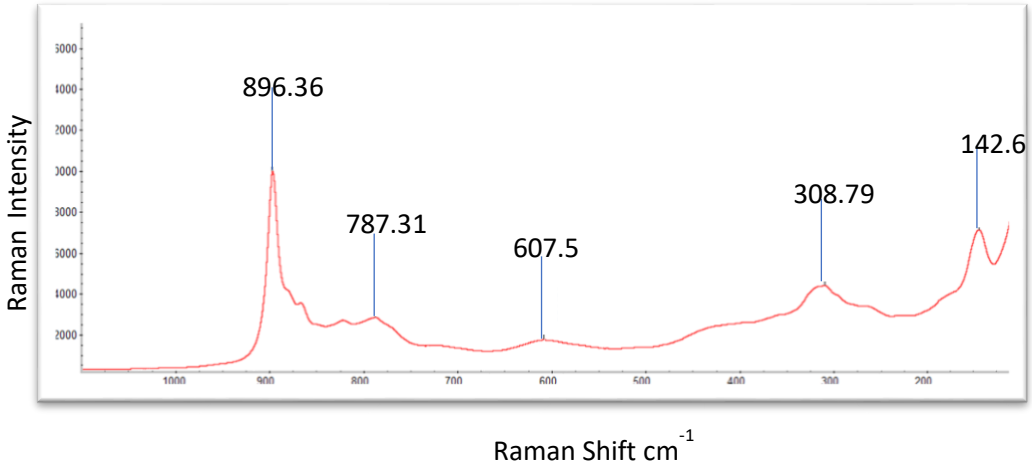

Figure 25: Raman Spectrum of the sample 1 (point 1)

Raman spectroscopy anaylysis has not been very successful with the majority of the samples. However, a few samples proved otherwise. The Raman spectrum produced from analysing the fly ash annealed at 350°C produced peaks that match closely with rutile and anatase peaks. From figure 25, 2 peaks that are of

interest at 607.57cm^{-1} and 142.67 cm^{-1}; corresponding to a rutile and anatase peaks respectively.

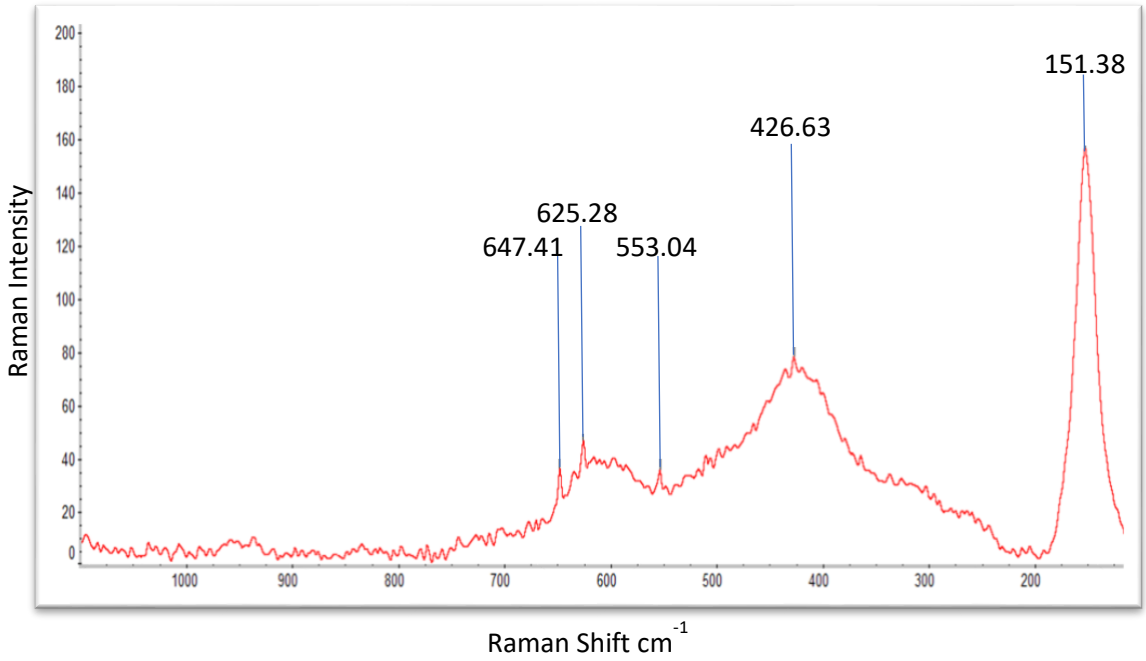

Figure 26: Raman spectrum from point 2 on sample 1

The Raman spectra on another area of focus on the same coated CFA (sample 1) gave rise to a slightly different pattern, figure 26, with an intense peak at 151.38cm^{-1}, which according to literature represents an anatase peak (Alemany et al., 2000)(Di Paola et al., 2013). Followed by a couple of broad peaks at 426.63 cm^{-1} and 625.28 cm^{-1} these two peaks correspond with rutile peaks. Hence, one can deduce that on this same batch of coated CFA both phases of TiO_2 coatings are present.

The characterisation of the coated CFA is not straightforward. The nature of the sample (coated CFA) can be complex to analyse and give definitive results. Unlike coating on a flat surface, you can expect accurate results from studying different focus points with the same sample. Hence, several analytical techniques and experimental tests are used to determine the success of the coating process.

4.1.2 Dye Degradation results

The dye degradation results obtained were to an extent fruitful. Figure 27 is an illustration of the MB absorbance over a period of time. Sample 4 exhibited rather excellent results, with decrease in absorbance of 89% of the main peak at 664nm with MB. Simultaneously sample 4 was also used as a photocatalyst with MO, giving a decrease of 15.7% of the main peak at 464nm. Unfortunately the raw data can not be used to plot a graph due to the theft of device holding the raw data. The results are from notes made in the diary.

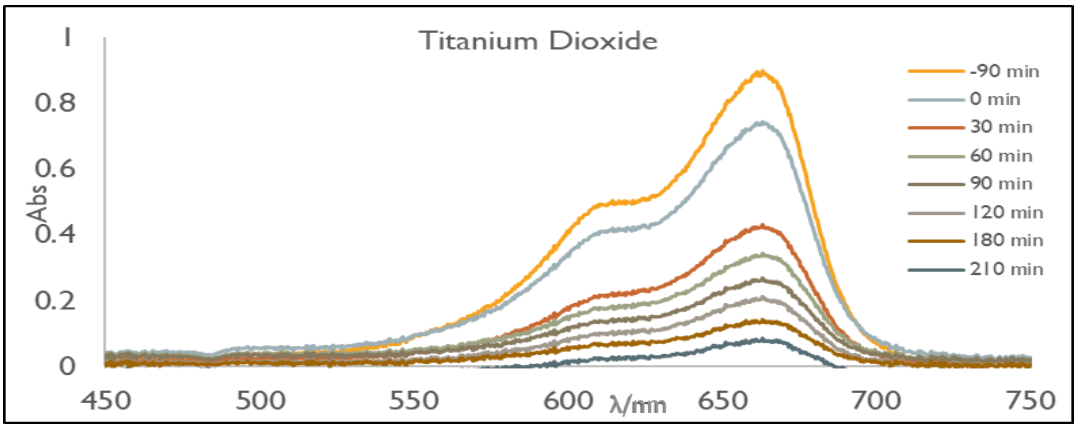

Figure 27: MB degradation under UV light

4.1.3 Desalinations results

The desalination process was conducted using two sources of water: seawater from Llandudno, North Wales and from a saltwater lake in Blackpool England. Both water samples have been tested for pH, turbidity, and conductivity. The premise of the experiment is that as desalination occurs the conductivity should decrease.

The desalination experiment was carried 6 times for the coated samples to confirm results and to ensure reproducibility. The pH and conductivity readings were carried in 4-hour intervals as illustrated in table 4.

Table 4: Conductivity and pH results from deslalination test using sample 5

	No CFA	Coated CFA	1hr	2hr	3hr	4hr
conductivity	38.4	38.7	36.3	36.1	36.1	45.5
pH	8.57	8.59	8.52	8.51	8.41	8.38

The obtained results in table 4 didn't correlate with reported results in the literature, Isha indicated a 25% decrease in salt concentration (Isha and Abd Majid, 2015). From the conducted experiments the conductivity was measured of the salt water before introducing sample 5 into the beaker and it was tested upon adding sample 5. The conductivity did not decrease as expected the conductivity reading at the start was 38.7mS/cm after 4 hours the reading was 45.5 mS/cm. Upon further discussion within the department, it was advised to test for longer duration. Based on the recommendation a run was conducted for a duration of 24hrs.Rreadings were recorded every hour for 8 hrs then a final reading the next day after 24hour; the results followed the trend as the previous experiments. The conductivity reading increased to 83.1 mS/cm. Following the results achieved a number of test were conducted using only CFA to help understand if the CFA has a negative impact on the desalination process. The results indicated that CFA is not responsible for any desalination activity nor results in the increase in conductivity as can been seen in table 5.

Table 5: Conductivity result of uncoated CFA 24hr period

Conditions	Start	24hrs
Dark	44.7ms	43.2ms
Under UV	44.9ms	43.3ms

4.1.4 Defluorination results

The experiment was carried in collaboration with the University of the Witwatersrad, South Africa, the fluoride experiment was conducted over a period of 3.50hours (210 minutes). Using sodium fluoride and deionised water to make the standards necessary to the following concentrations 100, 400, 800, 1200 and 1600 mg. L^{-1}. The standards made were used to calibrated the Orion meter used with a fluoride ion-selective electrode and a reference electrode. The log values of concentration versus mV graph from the results obtained were used to construct a calibration graph from which fluoride concentrations could be calculated.

The fluoride uptake of uncoated CFA was recorded to be 0.028mg/kg, this reading was recording as the benchmark for the fluoride uptake. The results recorded for the fluoride uptake of the TiO_2 bulk particles was recorded to be 35.59g/kg while on the other hand the recorded fluoride uptake of the sample 6, TiO_2 coated CFA was 32.20g/kg this indicates the reaction is truly a surface reaction and the bulk material doesn't effect the results much.

4.1.5 Acetone degradation

The results from the acetone degradation test, in the production of CO_2 did not comeback as anticipated. As mentioned earlier 5g of coated CFA with 3ml of acetone was used, the CO_2 concentration at the start was on average of 290ppm and remained at the same concentration of 290ppm with minimal fluctuations in

the readings over the test duration. Increasing the duration of the test did not affect the results. The concentration of the CO_2 in theory should increase as the activated TiO_2 breaks down the acetone to produce CO_2. This testing method was unsuccesfull even though different samples have been used including Samples 2,4 and 5.

4.2 Bismuth Titanium Oxide coatings deposited using large area rig

Figure 28 illustrates the XRD patterns from the uncoated CFA, sample 4 (TiO_2 coated CFA) and sample 7 ($BiTiO_x$ coated CFA). Comparing the patterns, one can see a distinct peak that may be attributed to bismuth.

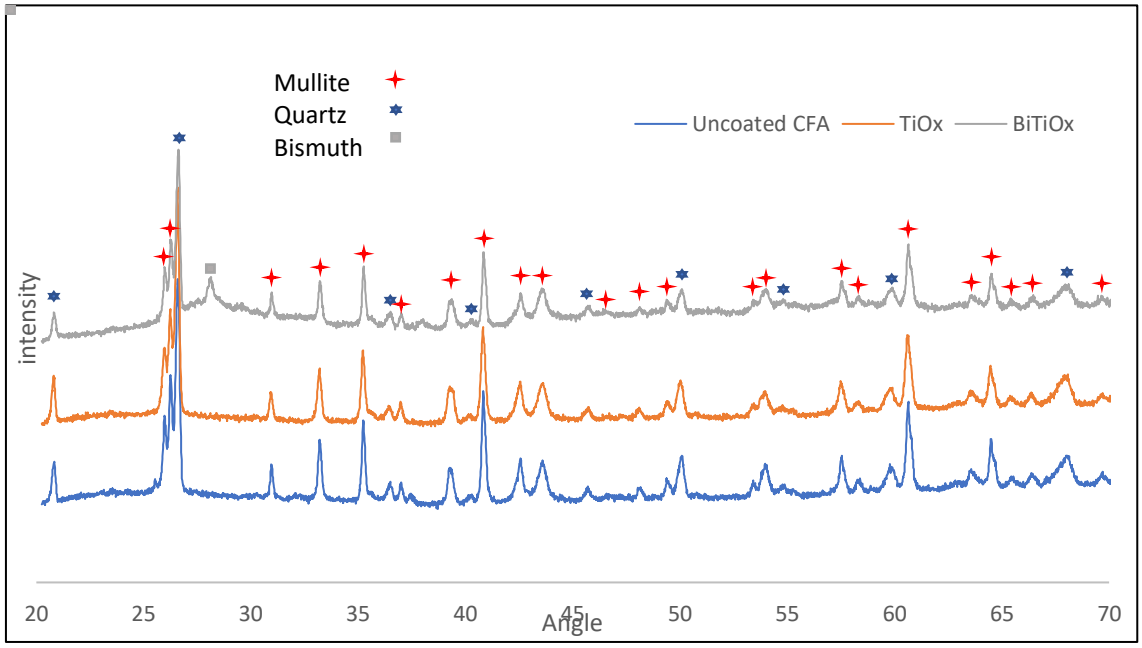

Figure 28: XRD patterns for uncoated CFA, sample 4 and sample 7

Further analysis has been conducted unfortunately the data can not be presented due to the theft of device holding the data.

For the $BiTiO_x$ coated CFA the precentag dye degradation percentage of 65.9% and 3.5%, from the main 664nm and 464nm peaks for MB and MO respectively. Thus, doping with Bismuth had a negative effect on photocatalytic performance,

as previous results for TiO_2 showed decreases of 89% and 15.7% for MB and MO respectively.

4.3 Deposition Bismuth Oxide using the small area rig.

The parameters used to coat CFA with bismuth oxide are listed in table 1, chapter 3.2.3. The majority of coated samples were unfortunately have been disposed off during building works in the laboratories. However, the characterisation using SEM EDX, XRD and XPS have been completed. Figure 29 illustrates the XRD pattern with distinct Bismuth oxide peaks. They peaks are attributed to Bi_2O_3 and Bi_4O_7 according to the XRD analysis.

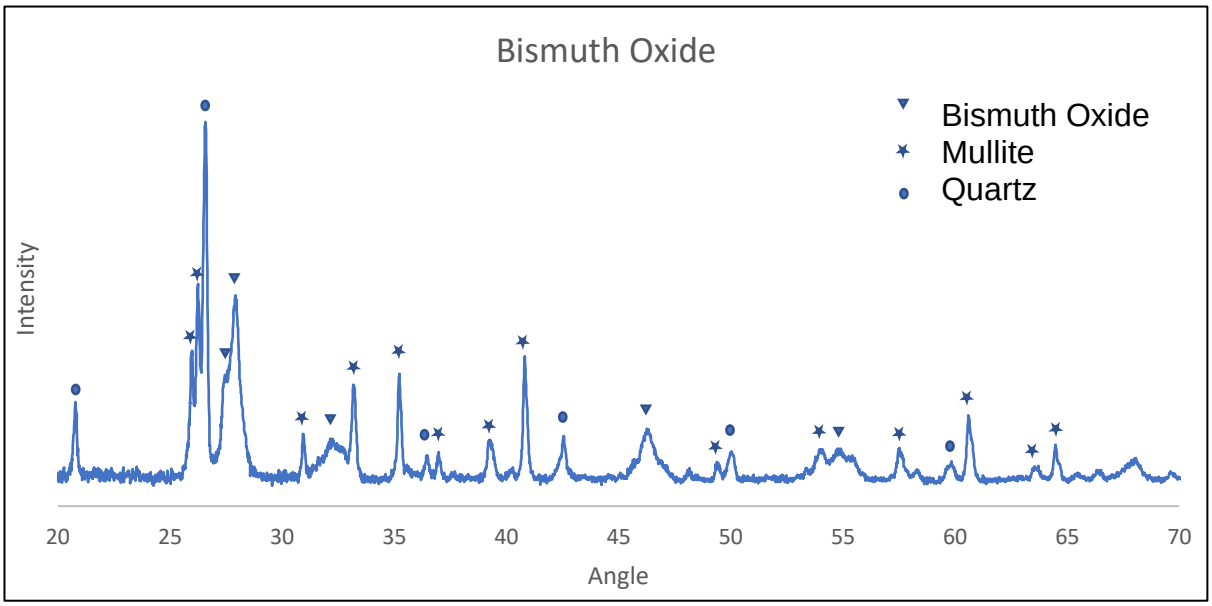

Figure 29: XRD pattern of bismuth oxide coated CFA - sample 8

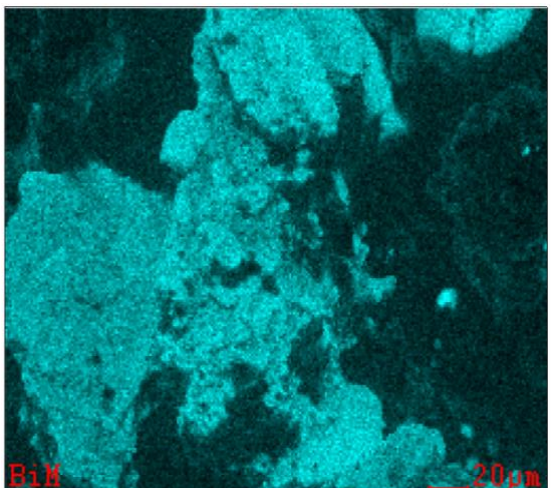

Figure 30: EDX mapping of sample 8

Table 6: EDX Wt% of sample 8

Element	Wt%	At%
CK	06.96	21.71
OK	13.23	31.00
NaK	00.08	00.13
AlK	13.78	19.14
SiK	12.33	16.45
BiM	49.96	08.96
CaK	00.78	00.73
TiK	00.35	00.27
FeK	01.40	00.94
CuK	01.14	00.67
Matrix	Correction	ZAF

Comparing the element composition of sample 8 (table 6) with uncoated CFA (table 1), one can see a clear difference with the presence of bismuth with an element composition of 49.96 wt%.

Sample 8 XPS analysis further confirms the successful deposition of Bi_2O_3 on to the surface of the CFA. Figure 31 illustrates the XPS narrow spectra of Bi_{4f} of the surface of the Bi_2O_3 coated CFA. The binding energies of $Bi_{4f\ 7/2}$ and Bi_{4f} 5/2 were observed to be 158.62 and 163.92 eV respectively. The binding energies were attributed to the Bi_2O_3 according to literature.

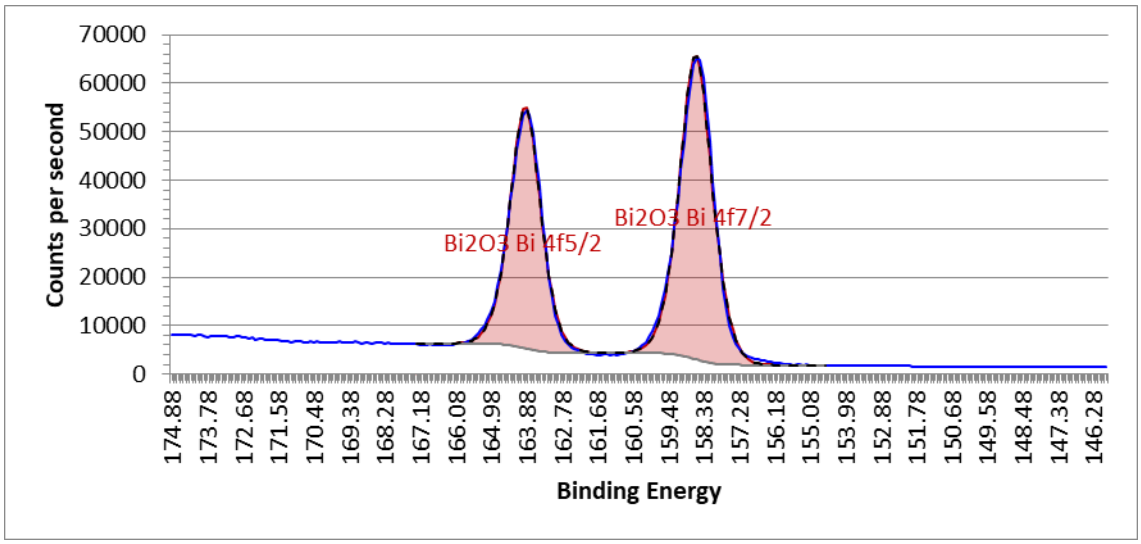

Figure 31: Sample 8 XPS narrow spectra

From literature it is noted that Bi_2O_3 as a photocatalyst is activated using visible light as mentioned in section 2.4.2. MB was degraded in the manner described in section 3.4.1 over a period of 180min using visible light.

From point of equilibrium at 0 min to 180min under visible light, a decrease in absorbance of 46.2% has been observed as depicted in figure 32. Which is lower than all the other coating variations adopted in this research for MB degradation.

With regards to acetone degradation the results were poor similar to the rest of the coating variations in this research.

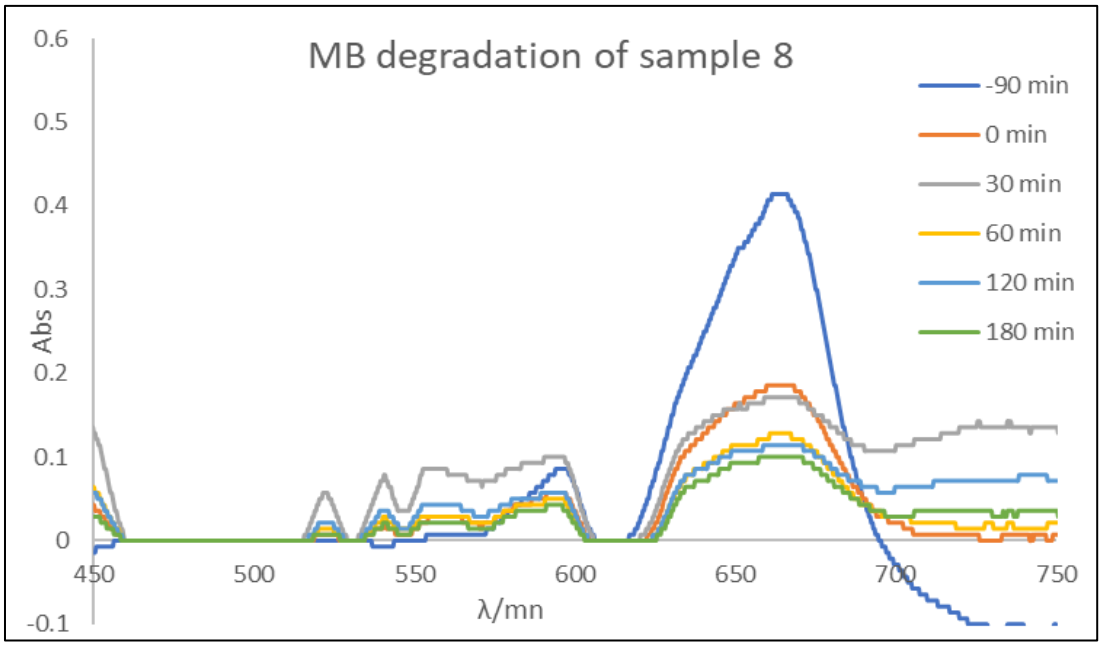

Figure 32: MB degradation of sample 8 in the presence of visible light

Figure 32 is an illustration of the MB absorbance over a period of 4.5 hours, 3 hours under visible light. Sample 8 exhibited good results results, with decrease in absorbance of 46.2% of the main peak at 664nm with MB. Incomparison to the results for TiO_2 showed decreases of 89% for MB. This finding indicates the ability of Bi_2O_3 coated CFA to be used in dye degradation. However, doesn't perform as well as a TiO_2 coated CFA.

4.4 Deposition of Titanium Dioxide onto glass beads

The glass beads supplied by ‘Sigma Aldrich’ are coated using the same method used in coating the CFA in the large area rig.The details of the coating parameters of sample 8 are included in table 1 in section 3.2.3. The reasoning behind coating glass beads are twofold. Firstly it is to compare a substrate with similar shape and composition of CFA which is silica, and how they perform when tested for dye degradation. Secondly, following a number failed photocatalyst tests namely the acetone degradation test to determine if the nature of CFA plays a role in effecting the results of the test.

The same procedures and techniques for analysis have used to analyse the coated glass bead.

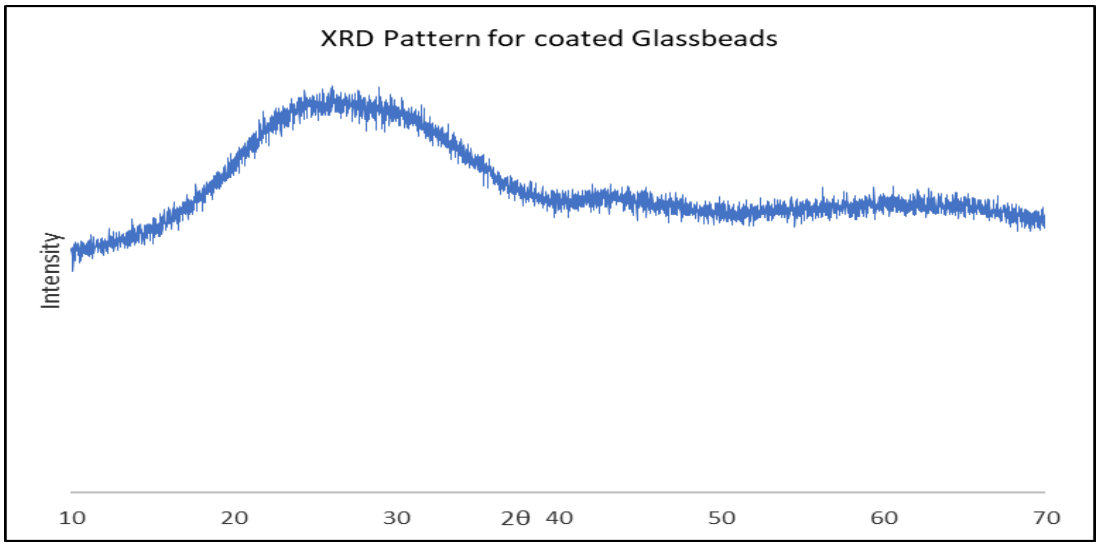

Figure 33: Sample 8 XRD pattern of TiO_2 coated glass beads

The XRD pattern came back with no diffraction peaks as illustrated in figure 33, even after annealing with different temperatures of the sample specimen and running it again.

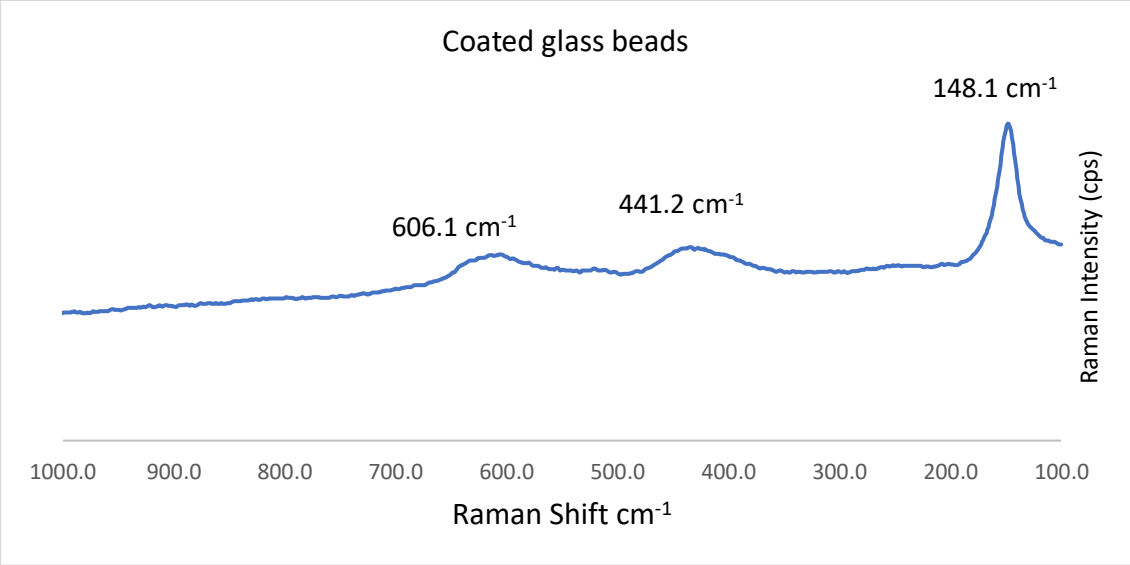

Figure 34: Raman Spectra of the coated glass beads at a specific point.

The XRF results came back with an increase in Ti mass percentage from 0.0145% to 4.44% indicating that titanium has been successfully deposited.

The Raman spectrum in figure 34 illustrates 3 distinctive peaks: 148.1cm^{-1}, 441.2cm^{-1} and 606.1cm^{-1}; the peaks correspond to sharp anatase peak and two broad rutile peaks, respectively.

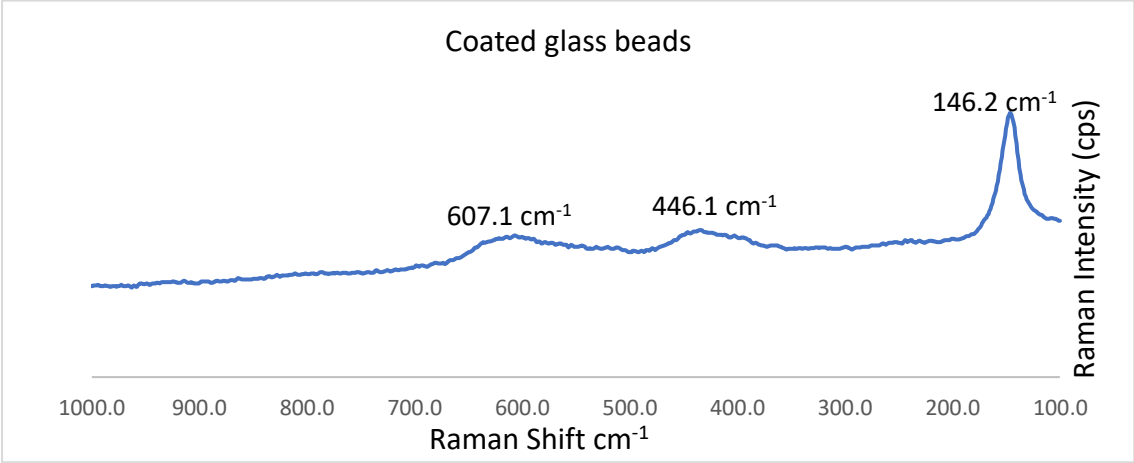

Figure 35: Raman Spectra of the coated glass beads at different point of the coated sample

Analysing a different point within the sample similar peaks as in figure 34 can be observed: a single peak at 146.1 cm^{-1} which corresponds to an anatase peak along with 2 broad rutile peaks at 607.1 cm^{-1} and 446.1 cm^{-1} as shown in the spectrum in figure 35.

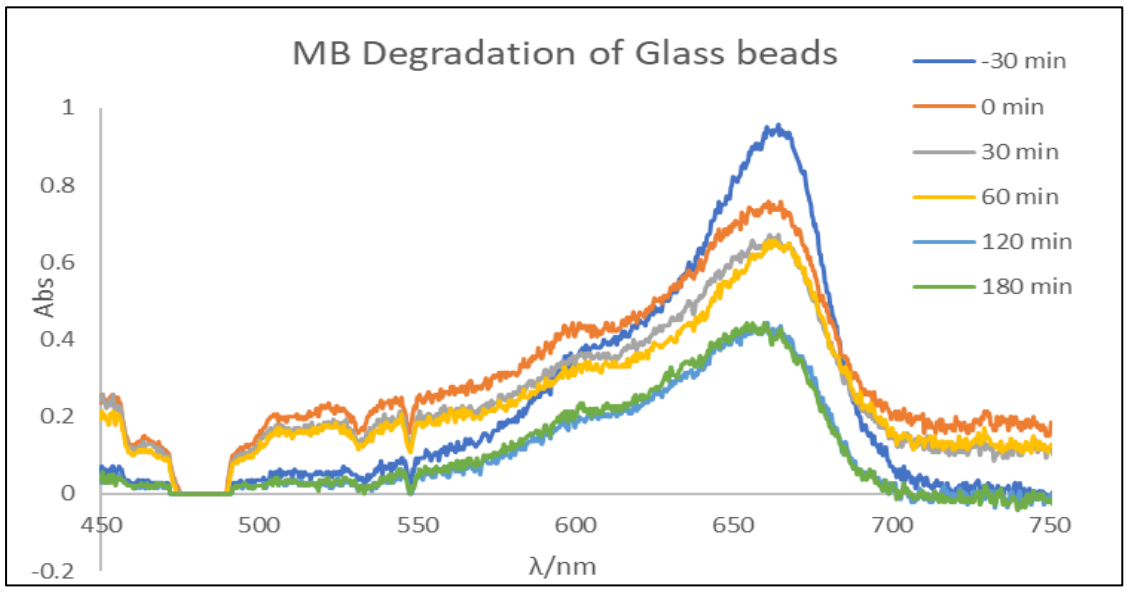

Figure 36: MB degradation graph of TiO_2 coated glass beads under UV

Figure 36 is an illustration of the change in MB absorbance over a period of 3.5 hours, with 3 hours under UV irradiation. Sample 9 exhibited good results, with a decrease in absorbance of 55.4% of the main peak at 664nm with MB. This is in comparison to the results for TiO_2 coated CFA, which showed decreases of 89% for MB. This finding indicates TiO_2 coated CFA is superior to TiO_2 coated glass beads, this may be attributed to utilising CFA as a substrate, which has substantially higher surface area than the glass beads.

5.0 Conclusion and further studies

The aim of the research was to utilise CFA as a substrate for photocatalytic coatings, and to investigate the effect and suitability in different environmental purposes. The research started with coating CFA with TiO_2 using the setup developed inhouse by the surface engineering group, before developing a suitable substrate holder for the purpose of the CFA particles. Upon coating the CFA with TiO_2, surface characterisation using XRD, XPS, SEM EDX, XRF and Raman spectroscopy was conducted. The characterisation results prove the successfull deposition of TiO_2 on to the surface of the CFA, XPS showed the presence of Ti $_{2p3/2}$ and $Ti_{2p1/2}$ which are attributed to TiO_2 from literature. Comparing the EDX data of uncoated CFA and TiO_2 coated CFA a significant increase in Ti wt% can be seen. The environmental applications have been successful to a degree, whereby photocatalytic dye degradation resulted in an decrease of absorbance by upto 89%. Furthermore, defluorination testing showed an fluoride uptake increase from 0.028mg/kg to 32.20g/kg between uncoated CFA and TiO_2 coated CFA respectively. However, the results of desalination and acetone degradation have not been as successful. Glass beads where introduced as a substrate to allow for a comparison due to its similar composition to CFA, and to help with understanding why certain environmental test didn't work as hoped. Unfortunately the acetone degradation test had the same poor results. Hence no further clarity was deduced to reasoning to this phenomenon.

Introducing another target to research with the aim to utilise visible light as an energy source for photocatalytic reaction bismuth was introduced to produce coating comprising of Ti and Bi. Surface characterisation was carried out, with

XRD and EDX data proving that bismuth was indeed deposited on the surface of the CFA. However, the photocatalytic performance of TiO_2 was superior in MB and MO dye degradation in comparison to $BiTiO_x$ coated CFA.

The use of the small rig was due to the circumstances with the large area rig not being available to due to demand, COVID and building works. The single target small rig was used to deposit Bi_2O_3 on to the surface of CFA which was succefully completed. Initially the aim was to determine the difference of photocatalytic performance between the different coated CFAs.

The research shows that indeed coated CFA may be utilised for environmental applications with great results achieved in MB degradation and fluoride uptake by TiO_2 coated CFA.

Further study is required to gain a deeper understanding of the reactions that take place with the coated CFA and to remodel the experimental set up and achieve better and more accurate results and reconsider certain parameters to allow for desired results to be achieved.

Nitrogen gas may be introduced to the system as a dopant, however, not yet explored in this research. This could be another angle to explore in further studies.

Bibliography

Ahamed, M. A. A., Perera, M. S. A., Matthai, S. K., Ranjith, P. G. and Dong-yin, L. (2019) 'Coal composition and structural variation with rank and its influence on the coal-moisture interactions under coal seam temperature conditions – A review article.' *Journal of Petroleum Science and Engineering*. Elsevier B.V., 180(June) pp. 901–917.

Ahmaruzzaman, M. (2010) 'A review on the utilization of fly ash.' *Progress in Energy and Combustion Science*, 36(3) pp. 327–363.

Alemany, L. J., Banares, M. A., Pardo, E., Martin-Jimenez, F. and Blasco, J. M. (2000) 'Morphological and Structural Characterization of a Titanium Dioxide System.' *Materials Characterization*, 44(99) pp. 271–275.

Ambroz, F., Macdonald, T. J., Martis, V. and Parkin, I. P. (2018) 'Evaluation of the BET theory for the characterization of meso and microporous MOFs.' *Small Methods*. John Wiley and Sons Inc.

Andricacos, P. C., Uzoh, C., Dukovic, J. O., Horkans, J. and Deligianni, H. (1908) *Damascene copper electroplating for chip interconnections*.

Andronic, L., Enesca, A., Vladuta, C. and Duta, A. (2009) 'Photocatalytic activity of cadmium doped TiO2 films for photocatalytic degradation of dyes.' *Chemical Engineering Journal*, 152(1) pp. 64–71.

Ashbolt, N. J. (2004) 'Microbial contamination of drinking water and disease outcomes in developing regions.' *Toxicology*. Elsevier, 198(1–3) pp. 229–238.

Bagheri, S., Muhd Julkapli, N. and Bee Abd Hamid, S. (2014) 'Titanium dioxide as a catalyst support in heterogeneous catalysis.' *Scientific World Journal*, 2014.

Beretta, G. P. (2007) 'World energy consumption and resources: an outlook for the rest of the century.' *International Journal of Environmental Technology and Management*. Inderscience Publishers, 7(1–2) pp. 99–112.

Bhangare, R. C., Tiwari, M., Ajmal, P. Y., Sahu, S. K. and Pandit, G. G. (2014) 'Distribution of natural radioactivity in coal and combustion residues of thermal power plants.' *Journal of Radioanalytical and Nuclear Chemistry*, 300(1) pp. 17–22.

Bhatnagar, A., Kumar, E. and Sillanpää, M. (2011) 'Fluoride removal from water by adsorption-A review.' *Chemical Engineering Journal* pp. 811–840.

Bhatt, A., Priyadarshini, S., Acharath Mohanakrishnan, A., Abri, A., Sattler, M.

and Techapaphawit, S. (2019) ‘Physical, chemical, and geotechnical properties of coal fly ash: A global review.’ *Case Studies in Construction Materials*. Elsevier Ltd., 11 p. e00263.

Bishop, C. A. (2007) *Vacuum deposition onto webs, films, and foils*. *Vacuum Deposition onto Webs, Films, and Foils*. William Andrew.

Brouwer, P. (n.d.) ‘THEORY OF XRF.’

Brundle, C. R., Evans, C. A. and Wilson, S. (1992) *Encyclopedia of materials characterization : surfaces, interfaces, thin films*. *Materials characterization series*.

Carlsson, J. O. and Martin, P. M. (2009) ‘Chemical Vapor Deposition.’ *In Handbook of Deposition Technologies for Films and Coatings: Science, Applications and Technology*. Elsevier, pp. 314–363.

de Castilho, B. C. N. M., Rodrigues, A. M., Avila, P. R. T., Apolinario, R. C., Nossa, T. de S., Walczak, M., Fernandes, J. V., Menezes, R. R., de Araújo Neves, G. and Pinto, H. C. (2022) ‘Hybrid magnetron sputtering of ceramic superlattices for application in a next generation of combustion engines.’ *Scientific Reports*. Nature Research, 12(1).

Coal & Electricity (n.d.).

Dehghanghadikolaei, A., Ansary, J. and Ghoreishi, R. (2018) ‘Sol-gel process applications: A mini-review.’ *Proceedings of the Nature Research Society*, 2 p. 02008.

Deraz, N. M. (n.d.) *The comparative jurisprudence of catalysts preparation methods: I. Precipitation and impregnation methods.*

Ding, J., Ma, S., Shen, S., Xie, Z., Zheng, S. and Zhang, Y. (2017) ‘Research and industrialization progress of recovering alumina from fly ash: A concise review.’ *Waste Management* pp. 375–387.

Dwivedi, A. and Jain, M. K. (2014) ‘Fly ash – waste management and overview : A Review.’ *Recent Research in Science and Technology*, 6(1) pp. 30–35.

EIA (2022) *Net electricity consumption worldwide in select years from 1980 to 2019 (in terawatt-hours)*. Statista. [Online] [Accessed on 15th February 2023] https://www.statista.com/statistics/280704/world-power-consumption/.

Emadzadeh, D., Lau, W. J., Matsuura, T., Rahbari-Sisakht, M. and Ismail, A. F. (2014) ‘A novel thin film composite forward osmosis membrane prepared from

PSf-TiO2 nanocomposite substrate for water desalination.' *Chemical Engineering Journal*, 237, February, pp. 70–80.

Fadleys, C. S. (2009) 'X-ray photoelectron spectroscopy: From origins to future directions.' *Nuclear Instruments and Methods in Physics Research, Section A: Accelerators, Spectrometers, Detectors and Associated Equipment*, 601(1–2) pp. 8–31.

Flewitt, P. E. J. and Wild, R. K. (2017) *Physical methods for materials characterisation, third edition*. *Physical Methods for Materials Characterisation, Third Edition*. CRC Press.

Fuentes, G. G. (2010) 'Surface Engineering and Micro-Manufacturing.' *In Micromanufacturing Engineering and Technology*. Elsevier, pp. 221–240.

FUJISHIMA, A. and HONDA, K. (1972) 'Electrochemical Photolysis of Water at a Semiconductor Electrode.' *Nature*, 238(5358) pp. 37–38.

Gamage, N., Liyanage, K., Fragomeni, S. and Setunge, S. (n.d.) 'OVERVIEW OF DIFFERENT TYPES OF FLY ASH AND THEIR USE AS A BUILDING AND CONSTRUCTION MATERIAL.'

Giurlani, W., Zangari, G., Gambinossi, F., Passaponti, M., Salvietti, E., Di Benedetto, F., Caporali, S. and Innocenti, M. (2018) 'Electroplating for decorative applications: Recent trends in research and development.' *Coatings*. MDPI AG.

Gohlke, J. M., Thomas, R., Woodward, A., Campbell-Lendrum, D., Prüss-Üstün, A., Hales, S. and Portier, C. J. (2011) 'Estimating the global public health implications of electricity and coal consumption.' *Environmental health perspectives*. National Institute of Environmental Health Sciences, 119(6) pp. 821–826.

Gottlieb, B., Gilbert, S. G. and Evans, L. G. (n.d.) 'Coal Ash A Report From physicians For social Responsibility And Earth Justice.'

Harris, N. S. (1989) 'Modern vacuum practice.' *London: McGraw-Hill*.

Hench, L. L. and West, J. K. (1990) *The Sol-Gel Process*. *Chem. Rev*.

Higham, E. H. and Paros, J. M. (2010) 'Measurement of Pressure.' *In Instrumentation Reference Book*. Elsevier Inc., pp. 145–163.

Hower, J. C., Senior, C. L., Suuberg, E. M., Hurt, R. H., Wilcox, J. L. and Olson, E. S. (2010) 'Mercury capture by native fly ash carbons in coal-fired power plants.' *Progress in Energy and Combustion Science*, 36 pp. 510–529.

Hvistendhal, M. (2007) *No TitleCoal Ash Is More Radioactive Than Nuclear Waste*.

Inspektor, A. and Salvador, P. A. (2014) 'Architecture of PVD coatings for metalcutting applications: A review.' *Surface and Coatings Technology*. Elsevier B.V., 257, October, pp. 138–153.

Isaacs, M. A., Davies-Jones, J., Davies, P. R., Guan, S., Lee, R., Morgan, D. J. and Palgrave, R. (2021) 'Advanced XPS characterization: XPS-based multi-technique analyses for comprehensive understanding of functional materials.' *Materials Chemistry Frontiers*. Royal Society of Chemistry, 5(22) pp. 7931–7963.

Isha, R. and Abd Majid, N. H. (2015) 'A Potential Hybrid TiO_2 in Photocatalytic Seawater Desalination.' *Advanced Materials Research*, 1113 pp. 3–8.

Iyer, R. S., Scott, J. A., Au, J. A. and Scott,) (2001) 'Power station fly ash — a review of value-added utilization outside of the construction industry.' *Resources, Conservation and Recycling*, 31 pp. 217–228.

Jagdale, P., Salimpour, S., Islam, M. H., Cuttica, F., Hernandez, F. C. R., Tagliaferro, A. and Frache, A. (2017) 'Flame Retardant Effect of Nano Fillers on Polydimethylsiloxane Composites.' *Journal of Nanoscience and Nanotechnology*, 18(2) pp. 1468–1473.

Jambhulkar, H. P., Shaikh, S. M. S. and Kumar, M. S. (2018) 'Fly ash toxicity, emerging issues and possible implications for its exploitation in agriculture; Indian scenario: A review.' *Chemosphere*. Elsevier Ltd pp. 333–344.

Kelly, P. J. and Arnell, R. D. (2000) 'Magnetron sputtering: A review of recent developments and applications.' *Vacuum* pp. 159–172.

Kovler, K. (2012) 'Does the utilization of coal fly ash in concrete construction present a radiation hazard?' *Construction and Building Materials*, 29 pp. 158–166.

Kumari, L., Lin, J. H. and Ma, Y. R. (2007) 'One-dimensional Bi2O3 nanohooks: Synthesis, characterization and optical properties.' *Journal of Physics Condensed Matter*, 19(40).

Li, D., Bulou, S., Gautier, N., Elisabeth, S., Goullet, A., Richard-Plouet, M., Choquet, P. and Granier, A. (2019) 'Nanostructure and photocatalytic properties of TiO2 films deposited at low temperature by pulsed PECVD.' *Applied surface science*. Elsevier, 466 pp. 63–69.

li, H. (2014) ‘Content and Distribution of Trace Elements and Polycyclic Aromatic Hydrocarbons in Fly Ash from a Coal-Fired CHP Plant.’ *Aerosol and Air Quality Research*, 14, January.

Li, H., Liu, G. and Cao, Y. (2014) ‘Content and distribution of trace elements and polycyclic aromatic hydrocarbons in fly ash from a coal-fired CHP plant.’ *Aerosol and Air Quality Research*, 14(4) pp. 1179–1188.

Luévano-Hipólito, E., Torres-Martínez, L. M. and Cantú-Castro, L. V. F. (2019) ‘Self-cleaning coatings based on fly ash and bismuth-photocatalysts: Bi2O3, Bi2O2CO3, BiOI, BiVO4, BiPO4.’ *Construction and Building Materials*, 220 pp. 206–213.

Luttrell, T., Halpegamage, S., Tao, J., Kramer, A., Sutter, E. and Batzill, M. (2014) ‘Why is Anatase a Better Photocatalyst Than Rutile? - Model Studies on Epitaxial TiO2 Films.’ *Scientific reports*, 4, February, p. 4043.

Manfredi, E. C., Flury, B., Viviano, G., Thakuri, S., Khanal, S. N., Jha, P. K., Maskey, R. K., Kayastha, R. B., Kafle, K. R. and Bhochhibhoya, S. (2010) ‘Solid waste and water quality management models for Sagarmatha National Park and Buffer Zone, Nepal.’ *Mountain Research and Development*. BioOne, 30(2) pp. 127–142.

Matthews, A. (2013) ‘Plasma Assisted PVD: The Past and Present.’ *SVC Bulletin* pp. 24–27.

Mattox, Donald M (2010) *Handbook of physical vapor deposition (PVD) processing*. William Andrew.

Mattox, Donald M. (2010) ‘Physical Sputtering and Sputter Deposition (Sputtering).’ *In Handbook of Physical Vapor Deposition (PVD) Processing*. Elsevier, pp. 237–286.

McBride, J. P., Moore, R. E., Witherspoon, J. P. and Blanco, R. E. (1978) ‘Radiological impact of airborne effluents of coal and nuclear plants.’ *Science (New York, N.Y.)*. United States, 202(4372) pp. 1045–1050.

Meenakshi and Maheshwari, R. C. (2006) ‘Fluoride in drinking water and its removal.’ *Journal of Hazardous Materials*, 137(1) pp. 456–463.

Mehrabadi, B. A. T., Eskandari, S., Khan, U., White, R. D. and Regalbuto, J. R. (2017) ‘A Review of Preparation Methods for Supported Metal Catalysts.’ *In Advances in Catalysis*. Academic Press Inc., pp. 1–35.

Mersagh Dezfuli, S. and Sabzi, M. (2019) ‘Deposition of ceramic nanocomposite coatings by electroplating process: A review of layer-deposition mechanisms and effective parameters on the formation of the coating.’ *Ceramics International*. Elsevier Ltd, 45(17) pp. 21835–21842.

Mitoraj, D., Lamdab, U., Kangwansupamonkon, W., Pacia, M., Macyk, W., Wetchakun, N. and Beranek, R. (2018) ‘Revisiting the problem of using methylene blue as a model pollutant in photocatalysis: The case of InVO4/BiVO4 composites.’ *Journal of Photochemistry and Photobiology A: Chemistry*, 366 pp. 103–110.

Mohapatra, M., Anand, S., Mishra, B. K., Giles, D. E. and Singh, P. (2009) ‘Review of fluoride removal from drinking water.’ *Journal of Environmental Management* pp. 67–77.

Musil, J., Baroch, P., Vlček, J., Nam, K. H. and Han, J. G. (2005) ‘Reactive magnetron sputtering of thin films: present status and trends.’ *Thin solid films*. Elsevier, 475(1–2) pp. 208–218.

Nayak, D. K., Abhilash, P. P., Singh, R., Kumar, R. and Kumar, V. (2022) ‘Fly ash for sustainable construction: A review of fly ash concrete and its beneficial use case studies.’ *Cleaner Materials*. Elsevier Ltd.

Oi, L. E., Choo, M. Y., Lee, H. V., Ong, H. C., Hamid, S. B. A. and Juan, J. C. (2016) ‘Recent advances of titanium dioxide (TiO2) for green organic synthesis.’ *RSC Advances*. Royal Society of Chemistry, 6(110) pp. 108741–108754.

Ojo, A. A. and Dharmadasa, I. M. (2018) ‘Electroplating of semiconductor materials for applications in large area electronics: A review.’ *Coatings*. MDPI AG.

Di Paola, A., Bellardita, M. and Palmisano, L. (2013) ‘Brookite, the Least Known TiO2 Photocatalyst.’ *Catalysts*, 3(1) pp. 36–73.

Pelizzetti, E. and Minero, C. (1993) ‘Mechanism of the photo-oxidative degradation of organic pollutants over TiO2 particles.’ *Electrochimica Acta*, 38(1) pp. 47–55.

Pouyfaucon, A. B. and García-Rodríguez, L. (2018) ‘Solar thermal-powered desalination: A viable solution for a potential market.’ *Desalination*. Elsevier B.V. pp. 60–69.

Rajoria, S., Vashishtha, M. and Sangal, V. K. (2022) ‘Treatment of electroplating

industry wastewater: a review on the various techniques.' *Environmental Science and Pollution Research*. Springer Science and Business Media Deutschland GmbH pp. 72196–72246.

Rao, V. V, Gosh, T. B. and Chopra, K. L. (1961) 'Vacuum Science and Technology.' *Physics Today*. Allied (First edition), 14(9) p. 88.

Ratova, M. (2013) *Enhanced Properties of Photocatalytic Titania Thin Films Via Doping During Magnetron Sputter Deposition*.

Ratova, M., Kelly, P. J., West, G. T., Tosheva, L. and Edge, M. (2017) 'Reactive magnetron sputtering deposition of bismuth tungstate onto titania nanoparticles for enhancing visible light photocatalytic activity.' *Applied Surface Science*. Elsevier, 392 pp. 590–597.

Ratova, M., Redfern, J., Verran, J. and Kelly, P. J. (2018) 'Highly efficient photocatalytic bismuth oxide coatings and their antimicrobial properties under visible light irradiation.' *Applied Catalysis B: Environmental*. Elsevier, 239(April) pp. 223–232.

Saepurahman, Abdullah, M. A. and Chong, F. K. (2010) 'Dual-effects of adsorption and photodegradation of methylene blue by tungsten-loaded titanium dioxide.' *Chemical Engineering Journal*, 158(3) pp. 418–425.

Saidur, R., Hasan, M. M., Haseeb, A. and Masjuki, H. H. (2008) 'Energy-efficient optical coating for flat glass.' *Journal of Applied Sciences*. Asian Network for Scientific Information, 8(10) pp. 1883–1890.

Sawtell, D. (2011) *Plasma enhanced chemical vapour deposition of silica thin films*. The University of Manchester (United Kingdom).

Sawtell, D., Martin, P. A. and Sheel, D. W. (2009) 'Enhanced AP-PE-CVD Process Understanding and Control by Application of Integrated Optical, Electrical and Modelling Diagnostics.' *Plasma Processes and Polymers*. Wiley Online Library, 6(S1) pp. S637–S642.

Sayilkan, F., Asiltürk, M., Tatar, P., Kiraz, N., Şener, Ş., Arpaç, E. and Sayilkan, H. (2008) 'Photocatalytic performance of Sn-doped TiO2 nanostructured thin films for photocatalytic degradation of malachite green dye under UV and VIS-lights.' *Materials Research Bulletin*, 43(1) pp. 127–134.

Seshan, K. (2002) *Handbook of thin-film deposition processes and techniques : principles, methods, equipment and applications*. Noyes Publications/William

Andrew Pub.
Shard, A. G. (2014) ‘Detection limits in XPS for more than 6000 binary systems using Al and Mg Kα X-rays.’ *Surface and Interface Analysis*, 46(3) pp. 175–185.
Shimizu, E., Promentilla, M. A. and Yu, D. E. (2020) ‘Utilization of Coal Fly Ash and Rice Hull Ash as System for Degradation of Dye in Wastewater.’ *Catalysts*, 10(2) p. 240.
SME (2021) ‘Coal’s Importance to the World,’ (February) pp. 1–8.
Solovyev, A. A., Rabotkin, S. V and Kovsharov, N. F. (2015) ‘Polymer films with multilayer low-E coatings.’ *Materials Science in Semiconductor Processing*. Elsevier, 38 pp. 373–380.
Son, D., Cho, S., Nam, J., Lee, H. and Kim, M. (2020) ‘X-ray-based spectroscopic techniques for characterization of polymer nanocomposite materials at a molecular level.’ *Polymers*. MDPI.
Sugama, T., Warren, J. and Butcher, T. (2011) ‘Self-degradable Slag/Class F Fly Ash-Blend Cements.’
Sullivan, J. J. (1985) ‘Development of variable capacitance pressure transducers for vacuum applications.’ *Journal of Vacuum Science & Technology A: Vacuum, Surfaces, and Films*. American Vacuum Society, 3(3) pp. 1721–1730.
Sushil, S. and Batra, V. S. (2006) ‘Analysis of fly ash heavy metal content and disposal in three thermal power plants in India.’ *Fuel*, 85(17–18) pp. 2676–2679.
Thoř, T. and Václavík, J. (2016) ‘Sol-gel preparation of silica and titania thin films.’ *In Optics and Measurement International Conference 2016*. SPIE, p. 101511A.
Torres-Huerta, A. M., Domínguez-Crespo, M. A. and López-Oyama, A. B. (2016) ‘Applications of CVD to Produce Thin Filmsfor Solid-State Devices.’ *Chemical Vapor Deposition: Recent Advances and Applications in Optical, Solar Cells and Solid State Devices*. BoD–Books on Demand p. 233.
Vassilev, S. V. and Vassileva, C. G. (2007) ‘A new approach for the classification of coal fly ashes based on their origin, composition, properties, and behaviour.’ *Fuel*, 86(10–11) pp. 1490–1512.
Verma, C., Madan, S. and Hussain, A. (2016) ‘Heavy metal contamination of groundwater due to fly ash disposal of coal-fired thermal power plant, Parichha, Jhansi, India.’ *Cogent Engineering*, 139.
Visa, M., Nacu, M. and Adrian, R. (2011) ‘Fly Ash Substrates for Complex

Wastewater Treatment.' *World*, 1.

Wang, N., Sun, X., Zhao, Q., Yang, Y. and Wang, P. (2020) 'Leachability and adverse effects of coal fly ash: A review.' *Journal of Hazardous Materials*, 396(January).

Wasa, K., Kitabatake, M. and Adachi, H. (2004) *Thin film materials technology: sputtering of control compound materials*. Springer Science & Business Media.

XRF Schematic (n.d.) (Oxford X-ray fluoresence 2009.

Yao, Z. T., Ji, X. S., Sarker, P. K., Tang, J. H., Ge, L. Q., Xia, M. S. and Xi, Y. Q. (2015a) 'A comprehensive review on the applications of coal fly ash.' *Earth-Science Reviews* pp. 105–121.

Yao, Z. T., Ji, X. S., Sarker, P. K., Tang, J. H., Ge, L. Q., Xia, M. S. and Xi, Y. Q. (2015b) 'A comprehensive review on the applications of coal fly ash.' *Earth-Science Reviews*. Elsevier pp. 105–121.

Yu, C., Zhou, W., Liu, H., Liu, Y. and Dionysiou, D. D. (2016) 'Design and fabrication of microsphere photocatalysts for environmental purification and energy conversion.' *Chemical Engineering Journal*. Elsevier B.V., 287 pp. 117–129.

Yu, X. and Shen, Z. (2011) 'Photocatalytic TiO 2 films deposited on cenosphere particles by pulse magnetron sputtering method.' *Vacuum*, 85(11) pp. 1026–1031.

Yu, X. Z. and Shen, Z. G. (2015) 'Comparison of nickel-coated cenosphere particles fabricated by magnetron sputtering deposition and electroless plating.' *Indian Journal of Physics*, 89(5) pp. 489–494.

Yu, Y. T. (2004) 'Preparation of nanocrystalline TiO 2-coated coal fly ash and effect of iron oxides in coal fly ash on photocatalytic activity.' *Powder Technology*, 146(1–2) pp. 154–159.